To the Graduate Council:

I am submitting herewith a thesis written by Miles Anthony Henderson entitled "A Morphological and Geochemical Investigation of *Grypania spiralis*: Implications for Early Earth Evolution." I have examined the final electronic copy of this thesis for form and content and recommend that it be accepted in partial fulfillment of the requirements for the degree of Master of Science, with a major in Geology.

Linda C. Kah, Major Professor

We have read this thesis and recommend its acceptance:

Christopher M. Fedo

David B. Finkelstein

Accepted for the Council:

Carolyn R. Hodges
Vice Provost and Dean of the Graduate School

A Morphologic and Geochemical Investigation of *Grypania spiralis*: Implications for Early Earth Evolution

A Thesis Presented for the
Master of Science
Degree
The University of Tennessee, Knoxville

Miles Anthony Henderson
August 2010

Acknowledgments

First, I would like to thank Vibhuti Rai (University of Lucknow, India), Tian Lifu (Hebei College of Geology, China), James St. John (Ohio State University), Hans Hofmann (McGill University, Canada), and Julie Bartley (Gustavus Adolphus College) for donating samples for this study, and Shuhai Xiao (Virginia Polytechnic University) for mediating the transfer of samples from China. I would also like to thank Monty and Mary-Ellen Schnur, who graciously provided access to the Greyson Shale fossil locality – your generosity toward generations of geologists has not gone unnoticed.

Thank you as well to the various agencies that have financially supported this research: the Belt Association, Sigma Xi, Geological Society of America Southeastern Section, and the Society for Sedimentary Geology (SEPM).

Finally, thanks to the University of West Georgia Microscopy Center (Julie Bartley), the University of Tennessee organic geochemistry laboratories (Dave Finkelstein), the University of Tennessee palynological laboratories (Sally Horn), and the High Temperature Materials Laboratory at Oak Ridge National Laboratory (Ed Kenik) for access to facilities and their support in operating analytical equipment.

Finally, I thank my wife, Viktoria, without whose support I would not have been able to complete this thesis research.

Dedication

This thesis is dedicated to the late Hans Hoffman, whose untimely death in May 2010 will be felt by many. May the degree of dedication with which Hans approached difficult questions regarding Proterozoic fossils and dubiofossils be a lesson to us all.

Abstract

Macroscopic "carbonaceous" fossils such as *Grypania*, *Katnia*, *Chuaria*, and *Tawuia* play a critical role in our understanding of biological evolution in the Precambrian and their environmental implications. Unfortunately, understanding of these fossils remains limited by their relative simplicity of form, mode of preservation, and broad taphonomic variability. As a result, debate continues as to even the fundamental taxonomic affinity of the organisms. Megascopic coiled forms (i.e. *Grypania* and *Katnia*), for instance, have been interpreted as trace fossils, multicellular algae, prokaryotic filaments, macroscopic bacteria, cyanobacteria, or a transitional form from macroscopic to megascopic bacterial life. Similarly, *Chuaria* and *Tawuia* have been interpreted as compressed prokaryotic colonies, algae or algal reproductive stages, and multicellular plant material. Accessibility of new material and increasingly sophisticated means of analysis warrant a new look at these ancient fossils.

Understanding the biological affinity of *Grypania,* in particular, is critical because current opinion is split as to whether these megascopic structures are more likely represent either multicellular bacteria or multicellular algae. Confirmation of either a bacterial or algal affinity would strongly influence fundamental understanding of biospheric evolution, particularly in terms of ocean oxygenation and the availability of bioessential trace metals. Although estimates for the degree of oxygenation required for a *Grypania*-like multicellular algae are only about 10 % present atmospheric levels (PAL), this estimate is still substantially higher than estimates based on geochemical data suggesting that oxygen levels may not have reached 10% PAL until the latter Neoproterozoic. It has been hypothesized that protracted oxygen of the Proterozoic biosphere may have played a critical role in the availability of redox-sensitive nutrients necessary for bacterial nitrogen fixation and the limiting of eukaryotic evolution. Within this context, our understanding of the taxonomic affinity of *Grypania* may profoundly affect our understanding of Earth's biospheric evolution. This thesis provides morphological and geochemical analyses of *Grypania spiralis* from more than 100 newly collected specimens from the Belt Supergroup for comparison to previously collected specimens from all other known *Grypania*-bearing localities. Data is used to explore questions regarding the morphology, structural complexity, mode of preservation, and chemistry of fossil material, and to hypothesize on the taxonomic affinity of *Grypania spiralis* and its implications for biospheric evolution.

Table of Contents

1. Introduction 1
2. Historical Context of Grypania Studies 3
3. Materials and Methods 6
   3.1 Sample Localities 6
      3.1.1 Greyson Shale – Belt Supergroup 6
      3.1.2 Gaoyuzhuang Formation – Changcheng System 10
      3.1.3 Rohtas Formation – Vindhyan Supergroup 10
      3.1.4 Negaunee Iron Formation – Marquette Range 11
   3.2 Analytical Methods 11
      3.2.1 Sample Collection 11
      3.2.2 Morphological Characterization 14
      3.2.3 *In Situ* Geochemical Characterization 16
      3.2.4 Ultrastructural Characterization 17
      3.2.5 Biochemical Characterization 18
4. Results and Interpretation 19
   4.1 Reconstruction of *Grypania* Morphology 19
      4.1.1 Morphologic and Taphonomic Characterization 19
      4.1.2 Morphological Interpretation 30
   4.2 Mode of Preservation 32
      4.2.1 Environmental Scanning Electron Microscopy – Secondary Electron Mode 32
      4.2.2 Environmental Scanning Electron Microscopy – Backscatter Electron Mode 35
      4.2.3 X-Ray Energy Dispersive Analysis (EDS) 35
      4.2.4 Interpretation of Preservation 36
   4.3 Ultrastructure of *Grypania* 47
      4.3.1 Ultrastructural Interpretation 47
   4.4 Biochemistry of *Grypania* 47
      4.4.1 Coulometry 47
5. Discussion 49
   5.1 Biological Affinity of *Grypania* 49
   5.2 Environmental Implications of *Grypania* 52
6. Conclusions 53
References 55
Appendix 1: Field Images 65
Appendix 2: Low Power Microscopy 67
Appendix 3: Morphological Measurements 69
Appendix 4: Scanning Electron Microscopy 71
Appendix 5: Geochemistry 73
Vita 76

List of Tables

Table 1. Taxonomic names applied to *Grypania*-like fossils……4

Table 2. Annotations for *Grypania* specimens in this study……12

Table 3. Carbon concentrations recorded from *Grypania*-bearing shale……48

List of Figures

Figure 1. Example of "annulations" within *Grypania* spp. ……5
Figure 2. Generalized Stratigraphy of Sample Localities……8
Figure 3. Representative *Grypania* fossils from each locality……9
Figure 4. Outcrop exposure of the Greyson Shale……13
Figure 5. Morphometric measurements taken from *Grypania* specimens……15
Figure 6. Variation in coiling patterns……...21
Figure 7. Terminations of *Grypania* ribbons……21
Figure 8. Folding of *Grypania* ribbons ...……21
Figure 9. *Grypania* specimens with transverse annulations……..22
Figure 10. Surficial markings associated with *Grypania* ribbons……..……24
Figure 11. Affect of grain size on *Grypania* preservation……..……...25
Figure 12. Part and counterpart preservation……..……...25
Figure 13. Morphometric measurements of *Grypania* specimens……..……...27
Figure 14. Conceptual model for spheroidal *Grypania* organism……..……...29
Figure 15. Conceptual model for helical *Grypania* organism……...29
Figure 16. Surface area-to-volume ratios……..……30
Figure 17. ESEM images of *Grypania* ribbons……..……...33
Figure 18. Composite image of *Grypania* coil……..……....33
Figure 19. ESEM images of annulated specimens of *Grypania*……..…….....34
Figure 20. Backscatter Electron images of bright spots detected……..36
Figure 21. ESEM-EDS analysis of Surficial markings……..37
Figure 22. ESEM-EDS analysis of *Grypania* ribbons……..…….38
Figure 23. ESEM-EDS analysis of *Grypania* ribbons……..…….....40
Figure 24. ESEM-EDS analysis of *Grypania* ribbons……...41
Figure 25. Depositional model for *Grypania*……..……...45
Figure 26. *Grypania* impressions in thin section…….……..…46

1. Introduction

Macroscopic "carbonaceous" fossils such as *Grypania* (Walcott, 1899; Walter et al., 1976; Walter et al., 1990; Horodyski, 1993; Sharma and Shukla, 2009), *Katnia* (Kumar, 1995; Sharma and Shukla, 2009), *Chuaria* (Walcott, 1899; Hofmann, 1977; Amard, 1992; Vidal et al., 1993; Kumar, 1995; Talyzina, 2000; Dutta et al., 2006; Sharma et al., 2009), and *Tawuia* (Kumar, 2001; Vidal et al., 1993; Sharma et al., 2009) play a critical role in our understanding of biological evolution in the Precambrian and their environmental implications. Multicellularity (Butterfield, 2000), colonialism (Neilson, 2006), macroscopic size (Payne et al., 2009), and molecular composition (Hedges, 2004) have implications for biologic evolution, the chemistry of the marine biosphere (O_2, CO_2, nutrients), and patterns of sedimentation. Unfortunately, understanding of these fossils remains limited by their relative morphological simplicity (Kumar, 2001), mode of preservation (Lamb et al., 2007, Orr et al., 2009), broad taphonomic variability (Samuelsson and Butterfield, 2001; Butterfield, 2003), and the current paucity of biochemical information (Arouri et al., 1999; Dutta et al., 2006; Sharma et al. 2009).

As a result, debate continues as to even the fundamental taxonomic affinity of these organisms. Megascopic coiled forms (i.e. *Grypania* and *Katnia*), for instance, have been interpreted as trace fossils (Walcott, 1899), multicellular algae (Du et al., 1986; Walter et al., 1990; Han and Runnegar, 1992, Horodyski, 1993), prokaryotic filaments (Vidal, 1989; Samuelsson and Butterfield, 2001), macroscopic bacteria (Glaessner, 1987), cyanobacteria (Sharma and Shukla, 2009), or a transitional form from macroscopic to megascopic bacterial life (Srivistava and Bali, 2006). Similarly, *Chuaria* and *Tawuia* have been interpreted as compressed prokaryotic colonies (Sun, 1987), algae (Zhang and Walter, 1992; Vidal et al., 1993), algal reproductive stages (Vidal et al., 1993), and multicellular plant material (Kumar, 2001).

Despite these uncertainties, there is little reason to question the biogenicity of these enigmatic structures. *Chuaria*, for instance, commonly preserves morphologies characteristic of compression of a spherical form (Sun, 1987; Kumar, 2001; Shukla et al., 2009), and organic remains have been successfully macerated from the rock matrix for ultrastructural and geochemical characterization (Dutta et al., 2006). Similarly, large size, coiling habit, overlapping of coils, and occasional occurrence of elements transverse to the ribbon length have long been interpreted as reflecting biogenicity in *Grypania* (Walter et al., 1990; Han and Runnegar, 1992;

Kumar, 1995; Sharma and Shukla, 2009), which is supported by the occasional concentration of carbonaceous material associated with the fossil material (Walter et al., 1976; Horodyski, 1993).

Accessibility of new material and increasingly sophisticated means of analysis warrant a new look at these fossils. Potential analytical paths include size analysis (Schultz and Jorgensen, 2001), shape analysis (Mankiewitz; 1992; Kumar, 1995; Xiao and Dong, 2006), structural analysis (Javaux et al., 2002; Moczydlowska and Willman, 2009), scanning electron microscopy (SEM; Orr et al., 2006; Lamb et al., 2007; Orr et al., 2009), X-Ray energy dispersive analysis (EDS; Lamb et al., 2007; Orr et al., 2009), Raman analysis (Schiffbauer et al., 2007; Schopf and Kudryavtsev, 2009), Fourier transform infrared spectroscopy (FTIR; Marshall et al., 2007), biomarker analysis (Summons et al., 1988; Sherman et al., 2007), and ultrastructural TEM (Javaux et al., 2002; Lamb et al., 2007; Schiffbauer and Xiao, 2009).

Understanding the biological affinity of *Grypania,* in particular, is critical because these megascopic carbonaceous compressions most likely represent either multicellular (i.e. colonial or aggregate) bacteria (Samuelsson and Butterfield, 2001; Sharma and Shukla, 2009) or algae (Du et al., 1986; Walter et al., 1990; Han and Runnegar, 1992). Constraint on domain level taxonomic affinity for *Grypania* would strongly influence our understanding of biospheric evolution, particularly in terms of ocean oxygenation and the availability of bioessential trace metals (Anbar and Knoll, 2002; Buick, 2009). For instance if *Grypania* represents a multicellular eukaryotic alga, estimates for the degree of oxygenation are small (~10% PAL; Runnegar, 1991), however these estimates are significantly higher than both the minimum post-GOE oxygenation levels ($>1\times10^{-4}$) provided by isotopic measurement of $\delta^{33}S$ (Farquhar et al., 2000) and estimates derived from time-dependent changes in oceanic $\delta^{34}S$ (Kah et al., 2004; Hurtgen et al., 2002) and Fe-speciation trends (Canfield et al., 2008) that suggest oxygenation levels may not have reached 10% PAL until the late Neoproterozoic.

This thesis provides detailed morphological and geochemical analyses of *Grypania spiralis* from more than 100 newly collected specimens from the Belt Supergroup (USA), and compares them to previously collected *Grypania* from the Gaoyuzhuang Formation (China), the Vindhyan Supergroup (India), and the Negaunee Iron Formation (USA). Data is used to explore primary questions regarding the morphology, structural complexity, mode of preservation, and

chemistry of fossil material, and combines new and existing observations to hypothesize on the taxonomic affinity of *Grypania spiralis* and its implication for biospheric evolution.

2. Historical Context of *Grypania* Studies

Bedding plane features broadly referred to as *Grypania* include a variety of material described under a range of formal names (Table 1). The unifying characteristics of these disparate forms include their occurrence as unbranched, uniform width ribbons that are preserved as carbonaceous bodies, films, or faint colorations on bedding planes of Precambrian shales (Walter et al., 1990; Han and Runnegar, 1992; Horodyski, 1993; Sharma and Shukla, 2009). Unfortunately, these characteristics are insufficient to define the taxonomic affinity of *Grypania* and the presence of coiled, sinuous, cuspate, and straight forms (Walter et al., 1976, 1990) suggest that morphology alone may be insufficient to diagnose whether *Grypania* represents a single or multiple biological entities.

Taxonomic investigation of *Grypania* fossils has concentrated largely on morphologic details observable by reflected light microscopy. Through these observations Paleoproterozoic *Grypania* (~1.9 Ga) has been interpreted as algae (Han and Runnegar, 1992) and as composites of prokaryotic filaments (Samuelsson and Butterfield, 2001). Investigations of Mesoproterozoic *Grypania* (~1.4-1.6 Ga) have led to interpretations as trace fossils, (Walcott, 1899), algae (Du et al., 1986; Walter et al., 1976; Walter et al., 1990), composites of prokaryotic filaments (Vidal, 1989), a transitional form from microscopic to megascopic life (Srivistava and Bali, 2006), and as cyanobacteria (Sharma and Shukla, 2009).

Additionally, several *Grypania* specimens exhibit evidence of elements transverse to the length of the ribbons (Fig. 1). These transverse elements have been interpreted as either a structural element of the organism sheath (Han and Runnegar, 1992), or as annulations that potentially represent cellular division (Sharma and Shukla, 2009). Furthermore, it has been suggested that coiled forms can be divided into two taxa, *Grypania spiralis* and *Katnia singhii*, based on the presence or absence of these annulations (Sharma and Shukla, 2009). At present, however, it is unclear to what extent this division aids in the taxonomic interpretation of *Grypania* because it is uncertain, even in well-preserved samples, whether annulations represent sheath ultrastructure (Han and Runnegar, 1992), bacterial cells within an undivided sheath

(Butterfield, 2009; Sharma and Shukla, 2009), or a differentiated eukaryotic sheath (Samuelson and Butterfield, 2001). Additionally, most annulated specimens (cf. Figures 4C, 4D, 6B, and 6D of Sharma and Shukla, 2009) appear to be highly degraded making the role of taphonomy in the origin of these features difficult to ascertain.

Table 1

Taxonomic Names applied to *Grypania*-like fossils.

Name	**Interpretation**	**Source**
Helminthoidichnites? spiralis	Metazoan Trace Fossil	Walcott, 1899
Helminthoidichnites meekii	Metazoan Trace Fossil	Walcott, 1899
Helminthoidichnites neihartensis	Metazoan Trace Fossil	Walcott, 1899
Grypania spiralis	Eukaryotic Algae	Walter et al. 1976
Proterania montania	Probably Algal	Walter et al. 1976
Katnia singhi	Annelid Remains	Tandon and Kumar, 1977
Spiroichnus beerii	Trace fossil	Mathur, 1983
Sangshuania sangshuanensis	Multicellular Algae	Du, Tian, and Li, 1986
Sangshuania linearis	Multicellular Algae	Du, Tian, and Li, 1986
Proterotania katniensis	Cyanobacteria	Sharma and Shukla, 2009

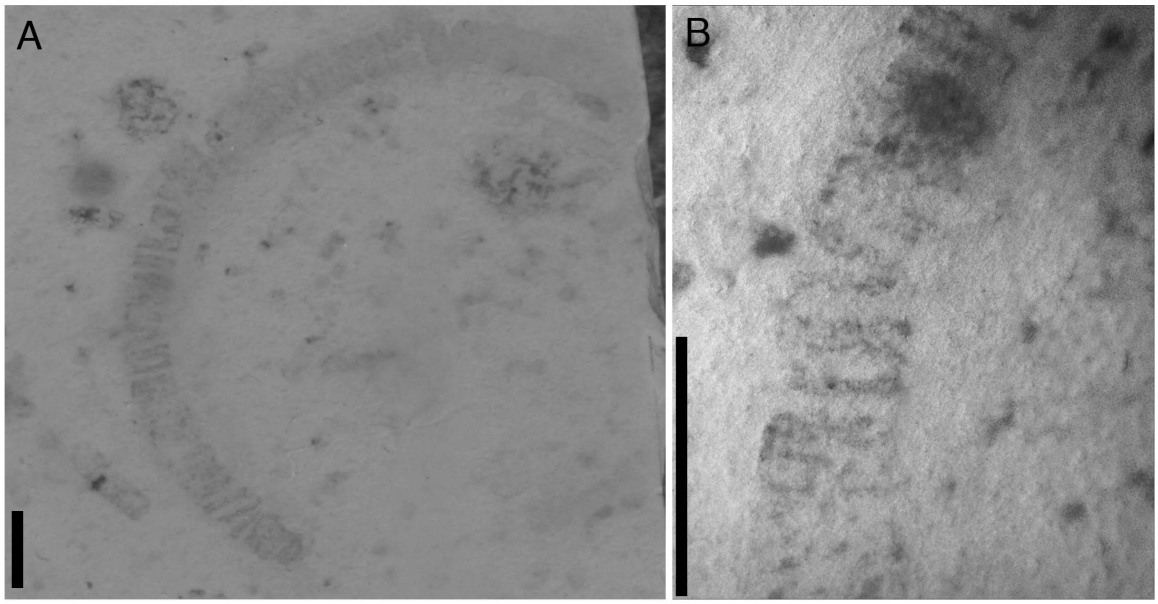


Fig. 1. Example of "annulations" within *Grypania* spp. (a) annulations, here from sample IND-L of the Rhotas Formation, India, occur as elements oriented transverse to the ribbon length; (b) detail of annulations from the same specimen, highlighting pairing of elements. Annulations have been considered to represent ultrastructural characteristics of an algal sheath (Han and Runnegar, 1992), transverse septae of an algal sheath (Kumar, 1995; Samuelson and Butterfield, 2001), and as individual cells within a bacterial trichome (Butterfield, 2009; Sharma and Shukla, 2009). Scale bars are 2 mm.

3. Materials and Methods

3.1 Sample Localities

Grypania spiralis has been identified from Paleoproterozoic and Mesoproterozoic rocks from the United States, China, and India (Fig. 2). Although *Grypania* is restricted to a single locality in the Paleoproterozoic (Negaunee Iron Formation, Marquette Range Supergroup, USA; Han and Runnegar, 1992), it has a much more geographically widespread occurrence in the Mesoproterozoic. Mesoproterozoic *Grypania* occurs in three localities, including the Greyson Shale (Belt Supergroup, USA; Walcott, 1899; Horodyski, 1993), the Gaoyuzhuang Formation (Changcheng System, China; Du et al., 1986; Walter et al., 2000), and the Rohtas Formation (Semri Group, Vindhyan Basin, India; Kumar, 1995; Sharma and Shukla, 2009). The generalized stratigraphy for each locality can be found in Figure 2, and representative examples from each locality are shown in Figure 3.

3.1.1 Greyson Shale – Belt Supergroup

The Belt Supergroup comprises a thick succession of sedimentary strata that extends from Western Montana into Idaho, Washington, and Canada and contains lithologies ranging from coarse conglomerates to arenaceous sandstone, to argillaceous shale, to impure calcitic and dolomitic carbonate (Harrison, 1972; Horodyski, 1993). Although organic remains are rare within the Belt Supergroup, two broadly contemporaneous units (the Greyson Shale and Appekunny Formation) contain macroscopic remains of putative eukaryotic origin (Horodyski, 1993). The occurrence of *Grypania* is restricted to within the Greyson Shale in the easternmost exposures of the Belt Supergroup in Montana, where it is exposed along an unpaved road approximately 100 m north of U.S. Highway 12. The Greyson Shale consists primarily of sub-greenshist stage olive-tinged, gray shale, muddy siltsone, and fine-grained sandstone that are interpreted to have been deposited in subtidal, offshore environments that progressively shallow upward in the section (Walter et al., 1990; Horodyski, 1993). The presence of rippled sandstone and flaser bedding within the fossil bearing horizons may suggest lower intertidal to subtidal environments for *Grypania* deposition.

The maximum age of the Greyson Shale is constrained by the plutonic basement rocks in southwestern Montana (1880-1860 Ma; Mueller et al., 2002) and mafic intrusions which intrude

Lower Belt strata and are dated at 1468 ± 2 Ma, 1469 ± 2.5 Ma, and 1457 ± 2 (U-Pb zircon; Zircon; Anderson and Davis, 1995; Sears et al., 1998). Younger mafic rocks within the Middle Belt Carbonate constrain the minimum age of the Greyson Shale at 1454 ± 9 (Sears et al., 1998). Together, these dates suggest *Grypania* within the Belt Supergroup to be early Mesoproterozoic in age.

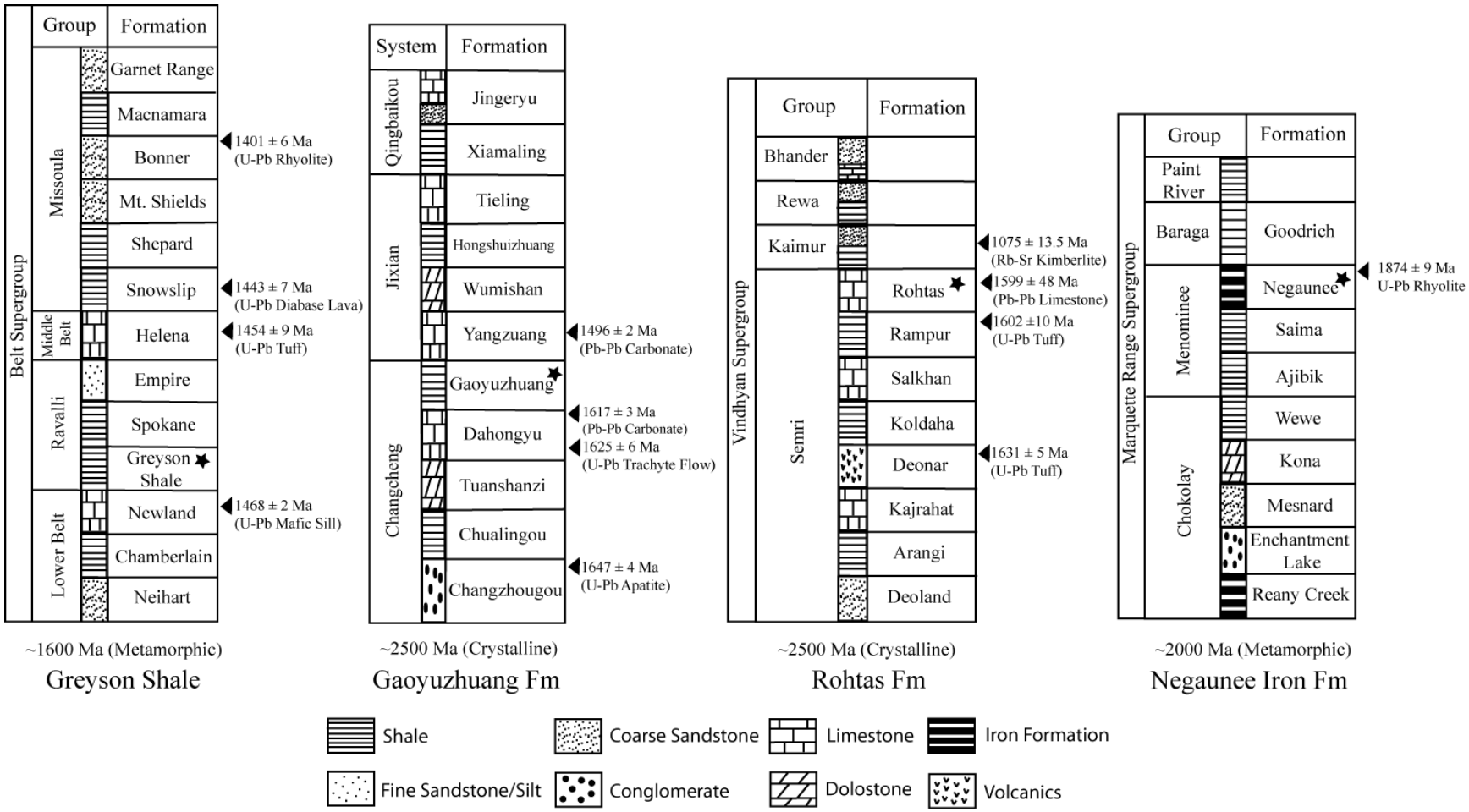


Fig. 2. Generalized stratigraphy of *Grypania* localities. Stratigraphy and lithologies are from (Walter et al., 1990; Horodyski, 1993, Sarangi et al., 2004; Sharma and Shukla, 2009); Radiometric age constraints are from (Crawford and Compston, 1970; Lu and Li, 1991; Walter et al., 1990; Jahn and Cuvellier, 1994; Anderson and Davis, 1995; Sears et al., 1998; Schneider et al., 2002; Ray et al., 2003; Sarangi et al., 2004; Gregory et al., 2006); Stars indicate the approximate location of *Grypania*-bearing units.

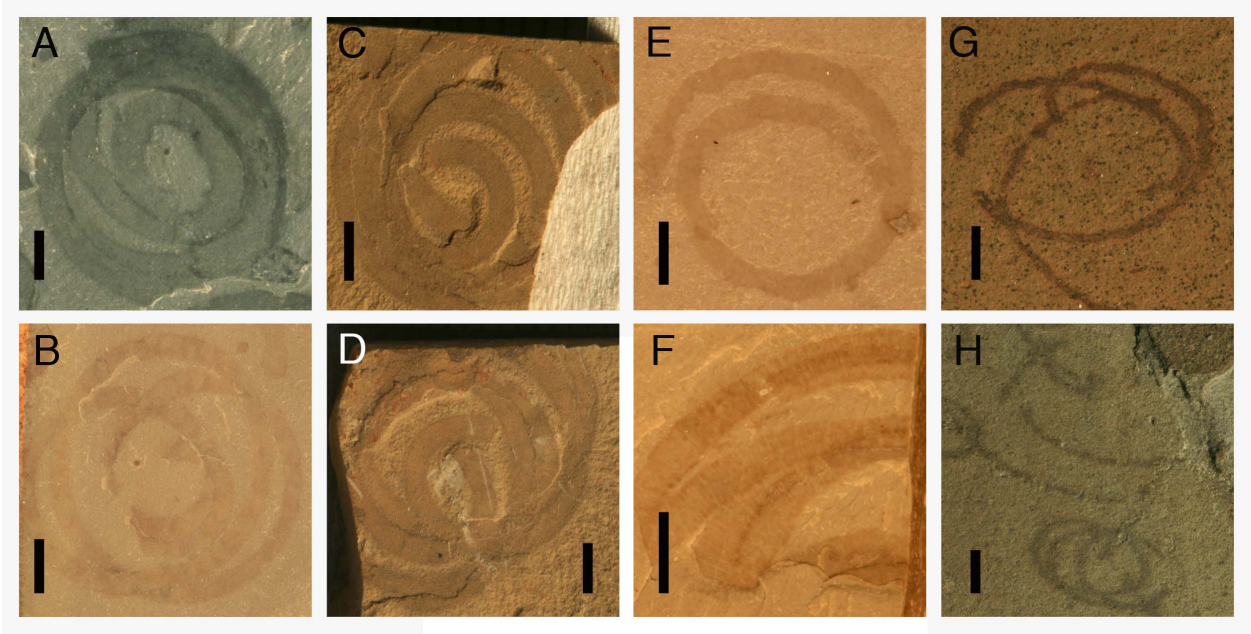


Fig 3. Representative *Grypania* fossils from each known locality. (a) Sample GS-PCZ and (b) Sample HH-1 from the Greyson Shale, Belt Supergroup, USA; (c) Sample GAO-7 and (d) Sample GAO-8 from the Gaoyuzhuang Formation, China; (e) Sample IND-C and (f) Sample IND-A from the Rohtas Formation, India; (g) Sample NG-1 and (h) Sample NG-2 from the Negaunee Iron Formation, USA. Scale bars are 2 mm.

3.1.2 Gaoyuzhuang Formation – Changcheng System

The Gaoyuzhuang Formation consists of fine sandstone, sandy shale, and muddy dolostone that crop out in the Jixian region in Northeast China (Hofmann and Chen, 1981; Du et al., 1985). *Grypania* occurs within green to dark gray to buff-colored marly dolostone and laminated mudstone that are interpreted to have been deposited in a subtidal lagoon protected from the ocean by a stromotolitic barrier bar (Walter et al., 1990).

The age of the Gaoyuzhuang Formation is clearly younger than the trachyte flow (1625 ± 6, U-Pb zircon; Lu and Li, 1991) near the top of the unconformably underlying Dahongyu Formation and younger than the youngest carbonate strata within this formation (1617± 3, Pb-Pb carbonate; Walter et al., 1990). Additional Pb-Pb dating of carbonate in the overlying Yangzhuang Formation provides an age of 1496 ± 82 Ma (Jahn and Cuvellier, 1994), which suggests that the Gaoyuzhuang Formation was deposited in the early Mesoproterozoic, between ~1600-1500 Ma. An early Mesoproterozoic age for *Grypania*-bearing strata is also consistent with stromatolite assemblages (Walter et al. 1990), C-isotopes stratigraphy of the overlying Jixian System (which suggests an age >1.3 Ga; Xiao et al., 2000). and preserved microfossil assemblages (Chen, 1985; Walter et al., 1990; Zhang, 2006).

3.1.3 Rohtas Formation – Vindhyan Supergroup

The Vindhyan Supergroup represents the largest exposure of Precambrian sedimentary rocks in central India. It consists of up to 4000 m of shale, sandstone, limestone, and dolostone with less abundant conglomeratic and volcanic rocks (Soni et al., 1987; Sarangi et al., 2004; Srivista and Bali, 2006). *Grypania* assemblages are found in the upper part of the Rohtas Formation near the town of Katni (Kumar, 1995; Sarangi et al., 2004). The interval in which *Grypania* is found consists of black to gray micritic limestone that grades upward into a carbonate-rich argillaceous succession that is interpreted to have been deposited in a low-energy, marine tidal flat (Kumar, 1995; Sarangi et al., 2004).

The Rohtas Formation is clearly younger than the Bundelkhand granite (2500 Ma), which comprises the basement for the Vindhyan Supergroup (Crawford and Compston, 1970; Kumar et al., 2001), and is also younger than a tuffs within the underlying Rampur Shale that have been dated at 1602 ± 10 (U-Pb zircon; Ray et al., 2003) and 1592 ± 12 (Gregory et al., 2006). The

upper age of the Rohtas Formation is constrained by a 1075 ± 13.5 Ma kimberlite intrusion (Gregory et al., 2006) that intrudes both Semri Group strata and the unconformably overlying Kiamur Group (Kumar, 1995; Sarangi et al., 2004). These bracketing ages are consistent with Pb-Pb dating of carbonate within the Rohtas Formation, which yields an age of 1599 ± 48 Ma (Sarangi et al., 2004).

3.1.4 Negaunee Iron Formation – Marquette Range Supergroup

The Marquette Range Supergroup consists of a thick successions of sedimentary strata that overlie the Superior craton in Northern Michigan and Wisconsin (Schneider et al., 2002). *Grypania* fossils occur approximately 200 meters above the stratigraphic base of the Negaunee Iron Formation within a succession of thinly bedded magnetite-carbonate-silicate- and chert (Han and Runnegar, 1992). Depositional models for the Negaunee Iron Formation suggest subtidal deposition on a stable shelf or subsiding passive margin (Schneider et al., 2002).

The age of the Negaunee Iron-Formation was determined by Sm-Nd radiometric dating to be approximately 2110 ± 52 Ma (Gerlach et al., 1988). U-Pb dating of a rhyolite in the laterally equivalent Hemlock Formation, however, provides an age of 1874 ± 9 Ma (Schneider et al., 2002), which is consistent with zircon ages of 1878 ± 1.3 Ma retrieved from a reworked volcanic ash in the broadly coeval Gunflint Formation in Ontario (Schneider et al., 2002). Until the Negaunee Iron Formation is directly dated it thus is reasonable to assume that it is not younger than ~1.85 Ga.

3.2 Analytical Methods

3.2.1 Sample Collection

In addition to previously collected samples of *Grypania* (Table 2), *Grypania* and associated shale were collected from the Greyson Shale during fieldwork in August 2009. Greyson Shale samples were collected for both morphologic and geochemical analysis and included samples from the exposed surface of the outcrop (Fig. 4) as well as from a depth of

Table 2.

Annotations for *Grypania* specimens used in this study.

Sample ID	Locality	Source
GAO	Gaoyuzhuang Formation, China	Tian Lifu, Hebei College of Geology
IND	Rohtas Formation, India	Vibhuti Rai, Lucknow University
NG	Negaunee Iron Formation, USA	James St. John, Ohio State University
HH	Greyson Shale, USA	Hans Hoffman, McGill University
BS	Greyson Shale, USA	Julie Bartley, Gustavus Adolphus College
GS*	Greyson Shale, USA	Current Study

***** Greyson Shale samples are additionally annotated with descriptors, which diagnose samples as containing full specimens (F), partial specimens (P), part and counterpart specimens (PC), uncoiled specimens (U), straight specimens (S), dendrites (D), and associated surficial material (M).



Fig. 4. Outcrop exposure of the Greyson Shale. (a) Fissile, highly jointed exposure of the Greyson Shale; (b) *Grypania* specimen on an exposed, weathered face of the Greyson Shale outcrop.

approximately 0.5 to 0.75 m into the outcrop. Samples were treated to avoid organic contamination during collection for geochemical analyses; freshly exposed, un-split shale was handled using nitrile gloves and placed into ashed aluminum foil. In the lab, samples were washed with deionized water and stored in ashed aluminum foil to await further preparation.

Samples used for morphologic investigation included more than 100 specimens from the Greyson Shale, 11 specimens from the Gaoyuzhuang Formation, 7 specimens from the Rohtas Formation, and 4 specimens from the Negaunee Iron Formation. Greyson Shale specimens included 63 specimens consisting of at least 1 full coil, 27 consisting of partial coils, and 23 specimens that show evidence of associated surficial markings.

3.2.2 Morphological Characterization

Reflected light microscopy and digital photography provided data for the morphological characterization and shape analysis of *Grypania*. Morphological characterization of *Grypania* included identification of style of coiling, presence or absence of annulations, morphology of terminal ends, and indications of ribbon contortion (e.g., folding, wrinkling, etc.) that provide information on the life form and taphonomy of the *Grypania* organism. Parameters for shape analysis included the number of preserved coils, ribbon width, ribbon length, coil diameter, and the arc length of the smallest and largest preserved coils (Fig. 5). *Grypania* coils that were measured from reflected light digital images using image analysis functions included with ImageJ64 software (available at http://rsbweb.nih.gov/ij/index.html). Frequency distributions for *Grypania* compiled for this study were binned using the zero stage rule of Wand (1997), where $h = 3.49\min(s, IQ/1.349)n^{-1/3,}$ where s is the sample standard deviation and IQ is the interquartile range. This methodology produces specified binning for each measured parameter in order to provide a smooth curve with maximum detail with respect to the sample population. Frequency histograms were plotted using the Paleontological Statistics (PAST) program (Øyvind Hammer; available at http://folk.uio.no/ohammer/past).

Scanning electron microscopy in secondary electron mode (ESEM-SED; Reed, 2005), was used to observe surface relationships between *Grypania* and surrounding matrix in order to investigate taphonomic processes involved in *Grypania* preservation. ESEM-SED imaging provides topographic information on the surface of the sample (Reed, 2005). ESEM was chosen because it

does not require specimens to be coated with gold or carbon prior to analysis, which preserves specimens for future geochemical analysis and avoids coating issues which have been suggested to have obscured morphological data during previous SEM attempts (Walter et al., 1976; Kumar, 1995).

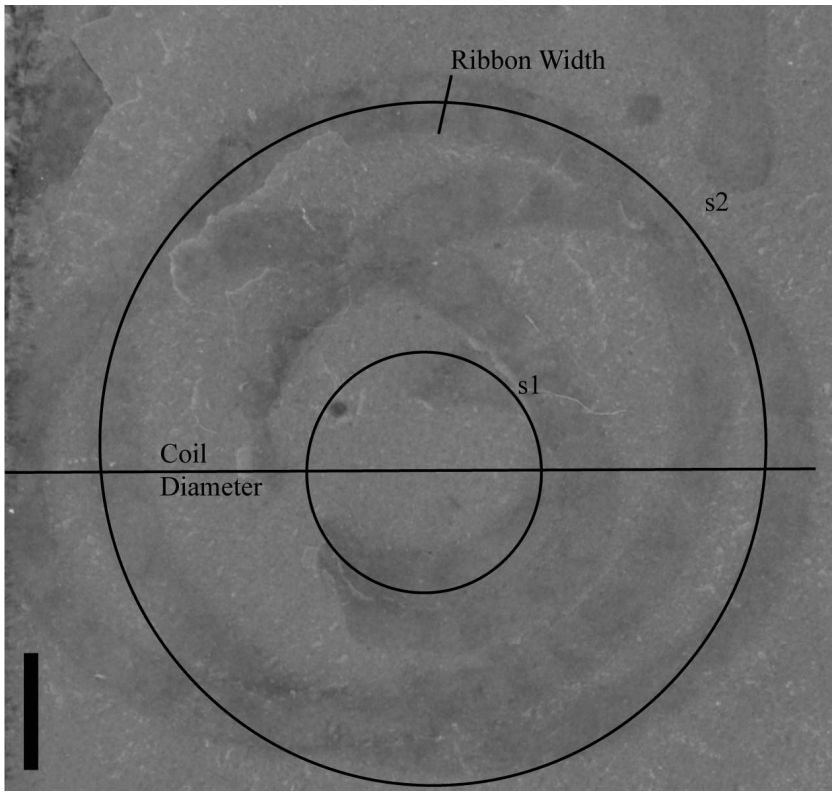


Fig. 5. Morphometric measurements taken on *Grypania* specimens. Measurements include ribbon width, ribbon length, diameter of the coil, and arc length of the smallest (s1) and largest (s2) coils. Coil measurements were obtained by finding the best-fit area of a circle, with arc lengths calculated using the circle radii with $\theta = 45$. The ratio of s1 to s2 produces an evaluation of the coiling tightness, where values near 0 are tightly coiled and values of 1 are loosely coiled. Scale bar is 2 mm.

Secondary electron imaging of *Grypania* ribbons was performed at the University of West Georgia using a Quanta 200 Environmental Scanning Electron Microscope. Seventy-eight samples of *Grypania* and *Grypania*-bearing shale were observed via ESEM at the West Georgia Microscopy Center at the University of West Georgia (UWG). In order to maximize the ability to recognize *Grypania* and surficial films with ESEM analyses were carried out at 10 kV (see Orr et al., 2009 for discussion). The chamber pressure was between 0.3 and 0.5 Torr at a distance of ~10 mm inside the vacuum chamber.

3.2.3 In Situ Geochemical Characterization

In situ geochemical characterization of *Grypania* and *Grypania*-bearing rock was performed using environmental scanning electron microscopy with backscatter detection (ESEM-BSD) and X-ray energy dispersive analysis (ESEM-EDS) to provide information regarding the potential differences in composition between preserved fossils and associated rock matrix. ESEM-BSD and ESEM-EDS of *Grypania*-bearing specimens were performed at the University of West Georgia using a Quanta 200 Environmental Scanning Electron Microscope.

ESEM-BSD provides compositional data on the sample analyzed. A voltage of 10 kV was used to observe *Grypania* ribbons in BSD mode in order to maximize the ability to detect both possible organic carbon and diagenetic products of organic matter, iron sulfides and manganese oxides. Backscatter detection mode (ESEM-BSD) on the ESEM uses high-energy electrons and a wide-angle detector (Reed, 2005). Because ESEM-BSD mode quickly discriminates between phases with higher atomic mass, the difference in atomic mass between carbon and common rock forming minerals (silicate and carbonate) produces a sharp contrast between organic matter and the surrounding rock matrix (Orr et al., 2002).

Elemental mapping with EDS allows for identification and quantification of elemental composition within matrix and fossils. For instance, preservation of non-mineralized carbonaceous material is rare and is commonly replaced by minerals that are nucleate and grow on an organic framework. Commonly, mineral templating includes the early diagenetic precipitation of pyrite (Briggs and Bartels, 2010) or the later diagenetic mobilization and precipitation of aluminosilicate clays (Lamb et al., 2007; Orr et al., 2009), either of which should be detectable with EDS. Elemental maps were produced from 250 frames of continuous data

collection at a voltage of 20 kV in order to get the most interaction of the electron beam with the sample surface for the range of elements analyzed to determine differences in elemental abundances within Grypania ribbons and the surrounding matrix. High-energy electrons interact with the surface producing characteristic X-rays with characteristic elemental spectra in ESEM-EDS (Reed, 2005). Although elemental mapping is most commonly applied to analysis of metazoan cuticle preserved on bedding planes (Orr et al., 2009), it been used successfully in the analysis of Precambrian carbonaceous compressions (Lamb et al., 2007). The interaction volume of the electron beam (X) used for mapping can be calculated by $X\ (\mu m) = 0.1E_0^{1.5}/\rho$, where E_o is the accelerating voltage (kV) and ρ is the rock density (g/cm^3). Low-energy X-ray maps are more likely to contain a significant topographic component than high-energy X-ray maps (Orr et al., 2009). To eliminate topographic components and obtain the greatest range of elements while restricting interaction volume, mapping of *Grypania* ribbons, associated surficial films, and surrounding matrix was carried out at a voltage of 20 kV. The interaction volume of X-rays, when calculated with a voltage of 20 kV and the average density for Greyson Shale (2.4 g/cm^3), is approximately 3.7 μm, which indicates that *Grypania* should be recognizable if mineralogical differences associated with its preservation are >3.7 μm in thickness.

Thin sections cut perpendicular to the bedding plane across *Grypania* ribbons were also analyzed via standard petrography and SEM-EDS in order to detect any potential mineralogical difference that may occur beneath *Grypania* ribbons. Similar techniques, including removing a cross section of a carbonaceous compression via focused ion beam (FIB) show promise in the characterization of the structure of Proterozoic organic walled fossils (Schiffbauer and Xiao, 2009), and potentially in the definition of mineralization associated with organic preservation. Ultrastructural characterization of *Grypania* cross sections was performed at Oak Ridge National Laboratory (ORNL) using a JEOL JSM-6500F field emission scanning electron microscope. Thin sections were coated with Ir and observed with an accelerating voltage of 5 kV to obtain suitably low interaction between the beam and the sample.

3.2.4 Ultrastructural Characterization

In order to assess the potential ultrastructure of organic material within *Grypania*-bearing samples, acid maceration was used to isolate organic constituents. *Grypania*-bearing shale from

the Greyson Shale was macerated using modified palynological techniques (Faegri and Iversen, 1975). Although palynological techniques are commonly employed for recovery of Precambrian microfossils, some researchers have had success in recovering macrofossils (Butterfield, 2000), and these methods have been successful in recovery of related macrofossils, such as *Chuaria* (Dutta et al., 2006). Approximately two grams of coarsely broken material was treated in 6N HCl overnight to remove carbonate phases, neutralized with a 10% KOH bath, and rinsed with distilled water. Samples were then treated in a 49% HF bath for 20 minutes then rinsed with hot alconox and distilled water. Samples were then treated in an acetic acid bath for 5 minutes, neutralized with a 5% KOH bath, and rinsed with distilled water. Macerates were transferred to vials and stained prior to slide preparation.

3.2.5 Biochemical Characterization

Finally, the content and composition of organic matter within *Grypania* and *Grypania*-bearing shale was assessed via organic carbon analysis and molecular characterization. Determination of molecular markers, in particular, may be a powerful tool for assessing the taxonomic affinity of Precambrian fossils (Brocks and Summons, 2003; Sherman et al., 2007) and has shown some promise in interpreting enigmatic "carbonaceous" structures such as *Chuaria* (Dutta et al., 2006).

Grypania-bearing shales were processed at the University of Tennessee for determination of organic carbon content. Specimens collected in the field were rinsed with DI water, dried, powdered using a stainless and Diamonite mortar and pestles, and homogenized. Approximately 80 mg of sample was weighed into 20 mL glass scintillation vials. Sample splits were exposed to an atmosphere of 6N HCl under vacuum for 48 hours (modified from Hedges and Stern, 1984) to remove carbon associated with carbonate minerals. Samples were then freeze-dried to remove any excess HCl and H_2O.

Grypania bearing rock from China and Montana was analyzed for organic and inorganic carbon with an automatic carbon dioxide coulometer. The automatic carbon dioxide coulometer performs a titration for CO_2, and when the endpoint is reached there is a registered color change that is recorded by a photometer and registered on the digital display (Huffman, 1977). Coulometric efficiency is 100% over long periods of time with a standard deviation of 0.02%.

Approximately 25 mg of acidified powdered sample was analyzed for organic carbon and another 25 mg of untreated sample was analyzed for carbonate carbon. Values are reported as the absolute percentage of inorganic or organic carbon, or total sample carbon.

4. Results and Interpretation

4.1 Reconstruction of Grypania Morphology

4.1.1 Morphologic and Taphonomic Characterization

Grypania fossils observed in this study are recognized as faint colorations on bedding planes. Although *Grypania* fossils are readily found at the outcrop surface, freshly split shale rarely contains the same concentration of *Grypania* fossils, suggesting that weathering may enhance the visibility of *Grypania* ribbons.

Grypania-like organisms are characterized by coiled, ribbon-like feature (i.e. flattened tubular structures, Han and Runnegar, 1992) that are uniform in width along a variable ribbon lengths. Although several occurrences reveal a straight or cuspate form, most of the study population exhibits variable coiling (Fig. 6) that is believed to represent compressed helices (Han and Runnegar, 1992). *Grypania* specimens exhibit both partial coils and full coils, single coils and doubly-terminated coils, ordered coils and disordered coils, coils that successively increase in diameter and those that retain similar coil diameter, and coils that overlap and those that show lateral displacement.

In addition to variable coiling, *Grypania* specimens also show variability in ribbon termination. Three shapes define the visible ends of *Grypania* ribbons: blunt, semi-rounded, and bulbous (Fig. 7). The vast majority of ribbons are represented by blunt, abrupt terminations that are interpreted as reflecting breakage of the ribbon. In only rare instances are *Grypania* ends preserved that are not broken, and in these cases, ends show either a semi-rounded termination or a broadening of the ribbon in a bulbous to triangular-shaped end. Although it is unclear whether broadening at the termination of Grypania is taphonomic in nature, such broadening is not uncommon in macroalgal holdfasts (Butterfield, 2000).

Finally, several *Grypania* specimens also show evidence for ribbon folding (Fig. 8) or the occurrence of structural elements transverse to the length of the ribbon (e.g., annulations; Fig. 9). Both ribbon folding and annulation of ribbons is diagnosed by a darkening of coloration on the

substrate similar as to that observed when ribbon coils overlap. Folding of ribbons—rather than coil overlapping—is most often observed in non-coiled specimens and in specimens that show disordered coiling (Fig. 8). By contrast, ribbon transverse elements, or annulations, most commonly occur in more tightly coiled forms. In the samples examined for this study, annulations occur on six specimens of *Grypania*, two from the Rohtas Formation, and four from the Greyson Shale (Fig. 9). Annulations occur as vague to distinct dark elements, with relatively even spacing down the length of the ribbon. Details of annulations, however, show substantial variation. Whereas some annulations appear as narrow, paired elements (Figs. 9a and a'; Figs. 9e and e'), others appear as broad, singular elements (Figs. 9b and b'; Figs. 9d and d'). Still other annulations appear as irregular elements with concave edges (Figs. 9c and c') or as indistinct blebs arranged along the length of the ribbon (Figs. 9f and f'). Variability in morphology of annulations may represent true biological distinctions (Sharma and Shukla, 2009), but may also represent taphonomic variability of the parent ribbons. Evidence for a strong taphonomic influence on annulation appearance is suggested even by differences in coloration, wherein specimens with darker ribbons typically preserved the most distinct annulations.

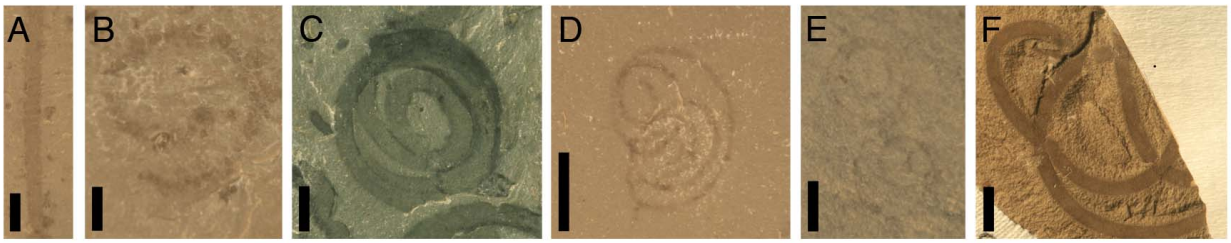


Fig. 6. Variable coiling patterns exhibited by *Grypania*. (a) Sample GS-U2 preserved as a straight ribbon; (b) example of a loose coil, sample GS-F27; (c) example of a tightly coiled specimen, sample GS-PCZ; (d) sample BS-A and (e) sample GS-F17 showing variation on doubly terminated coils; (f) disordered coils, sample GAO-2. Scale bars are 2 mm.

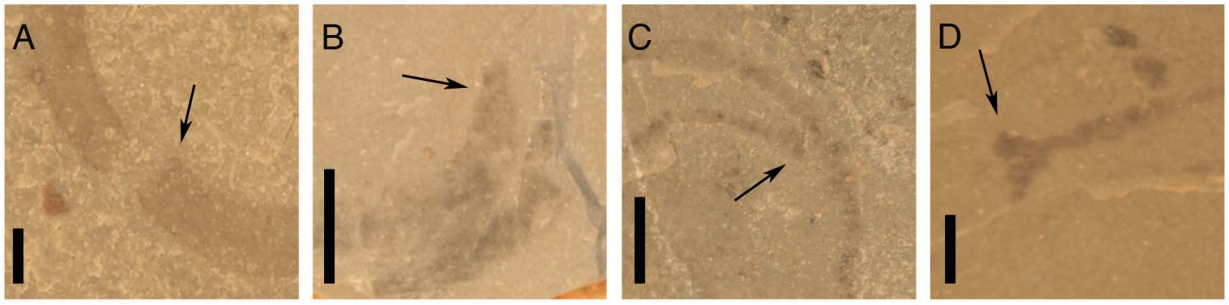


Fig. 7. Termination of *Grypania* ribbons. (a) Sample BS-C and (b) sample GS-P14 showing abrupt or blunt ends associated with ribbon fracture; (c) sample GS-F9 and (d) sample GS-F10 showing bulbous to triangular expansion of ribbon termination. Scale bars are 1 mm.

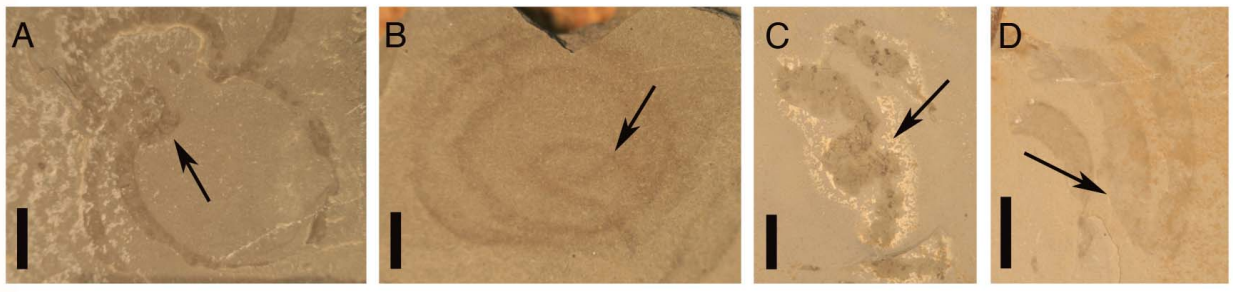


Fig. 8. Examples of folding in Greyson Shale *Grypania*. (a) Sample GS-F6, (b) sample GS-F20, (c) sample GS-P6, and (d) sample GS-P6. Arrows indicate folds. Scale bars are 2 mm.

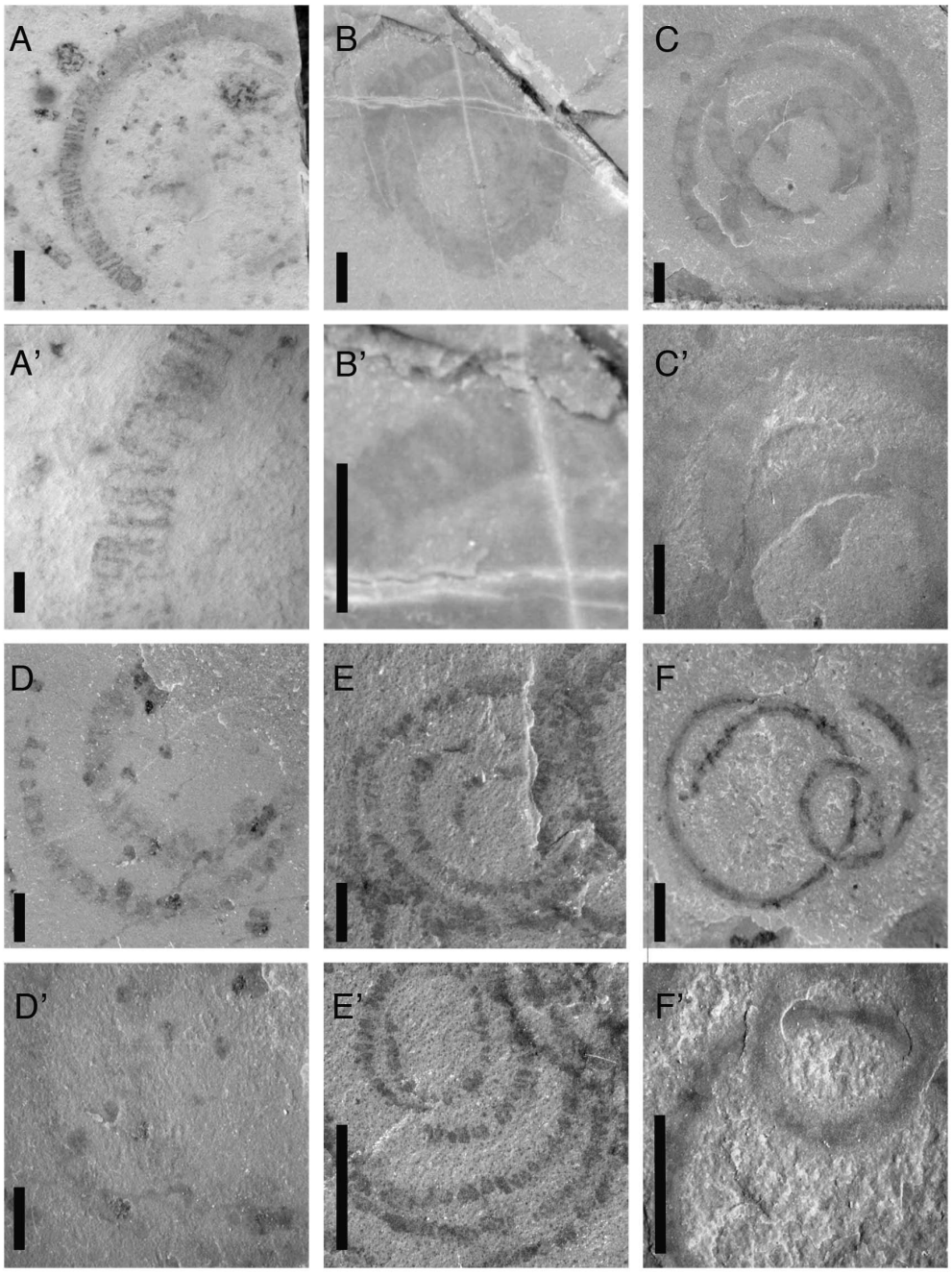


Fig. 9. *Grypania* specimens showing transverse annulations. (a and a') Sample IND-L and detail of narrow, paired elements; (b and b') sample IND-C and detail showing broad, singular elements; (c and c') Sample HH-1 and detail showing irregular, concave elements; (d and d') Sample GS-P11 and detail showing broad, singular elements; (e and e') Sample GS-F30 and detail of narrow, paired elements; and (f and f') Sample GS-PCL and detail of irregular dark patches. Scale bars are 2 mm.

In addition to *Grypania* fossils, a wide variety of other surficial markings are found within *Grypania*-bearing rocks (Fig. 10). These markings are most common throughout the Greyson Shale, although they are not found in abundance near *Grypania* coils. Films appear to have two distinct morphologies, one that appears as isolates, diffuse, string-like forms and the other that appears as small (1-2 mm) blebs that commonly covers larger areas of the shale surface. In some instances, bleb-like forms appear to be oriented in irregular arcs that potentially indicate their origin as a taphonomic breakdown of *Grypania* ribbons. Although the majority of surficial markings observed in this study occur in the Greyson Shale, similar markings were found on a single sample from the Gaoyuzhuang Formation; no films were found in association with *Grypania* samples from the Rohtas Formation or Negaunee Iron Formation.

It remains uncertain how much of observed variability in *Grypania* results from taphonomic variation. Taphonomic variation, however, cannot be discounted because several observations indicate that environmental controls play a substantial role in *Grypania* preservation. The quality and character of *Grypania* fossils clearly varies with both grain size of the rock matrix (Fig. 11) and whether fossils are recovered from a part or counterpart of the matrix material (Fig. 12). With respect to grain size, *Grypania* typically show a decrease in the definition of ribbons with increasing grain size from approximately 1 μm, wherein details of ribbon structure is most complete, to approximately 12.3 μm, at which point ribbon structure becomes exceedingly diffuse. Difference in grain size may also play a role in the variation observed between part and counterpart of split samples. Preservational differences between part and counterpart are common (Orr et al., 2009), with darker, more distinct features correlating well to the preferentially finer grained surface.

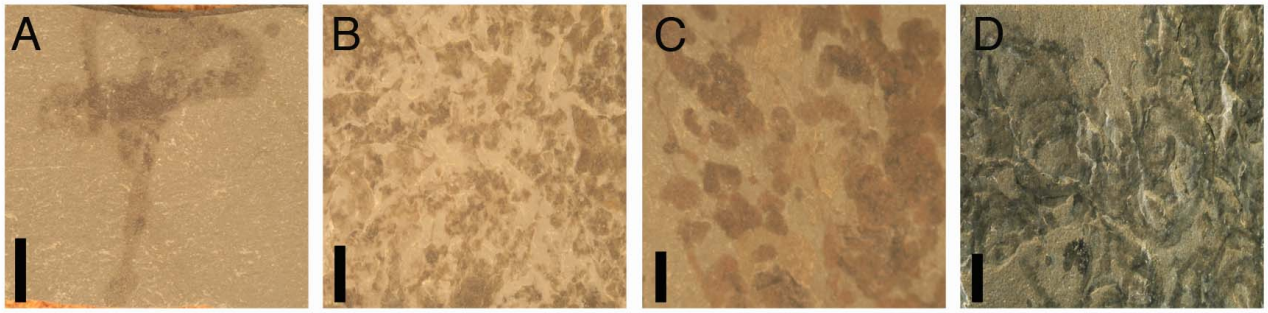


Fig.10. Surficial markings associated with *Grypania*. (a) Sample BS-D showing diffuse, stringy markings; (b) sample GS-M5 and (c) sample GS-F4 and (d) sample GS-F22 showing distinct, small blebs that appear oriented in accurate patterns that suggest a taphonomic end-member of *Grypania* ribbons. All samples are from the Greyson Shale. Scale bars are 2 mm.

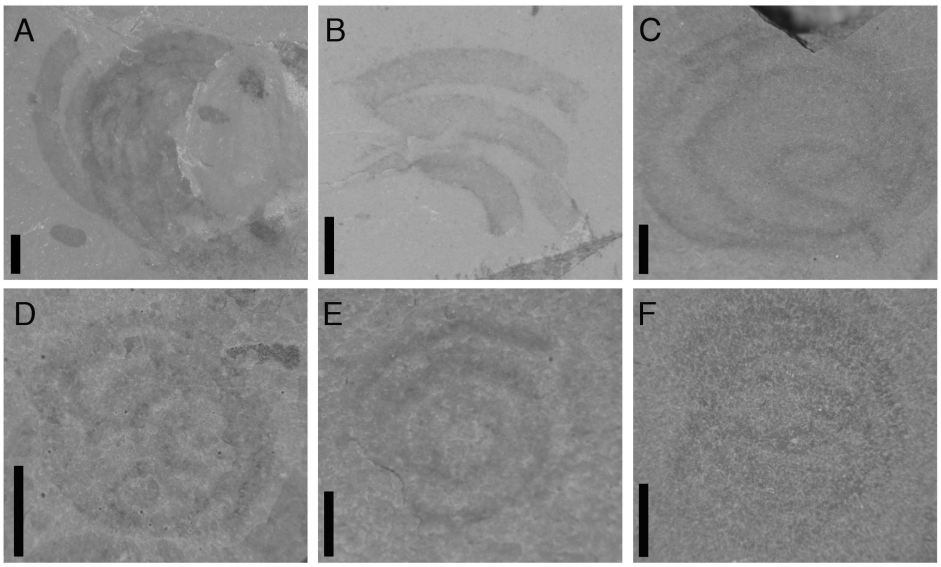


Fig. 11. Affect of grain size on the preservation of *Grypania* ribbons. An increase in grain size is typically correlated with a loss of distinction at ribbon edges, thinning and greater irregularity in ribbon width, and an increase in the patchiness of surficial coloration. (a) Sample GS-PCZ and (b) sample GS-P6 at 1 μm; (c) sample GS-F20 at 1.2 μm; (d) sample GS-F23 at 1.5 μm; (e) sample GS-F7 at 1.8 μm; (f) sample GS-F18 at 12.3 μm. Scale bars are 2 mm.

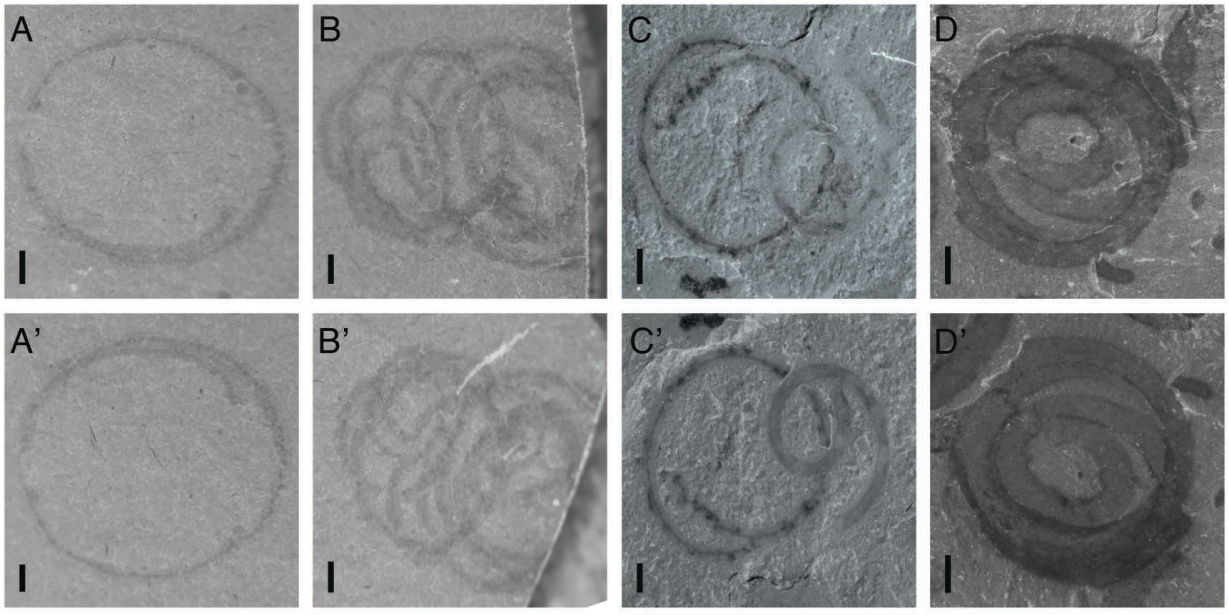


Fig. 12. Part and counterpart preservation of *Grypania* ribbons. Differences in grain size and preferential distribution of organic material are commonly observed in parts and associated counterparts. (a and a') Sample GS-PCK; (b and b') sample GS-PCJ; (c and c') sample GS-PCL; (d and d') sample GS-PCZ; Scale bars are 2 mm.

Measurements of Grypania included ribbon width, ribbon length, the number of coils, and the relative tightness of coiling (Fig. 13). Individual ribbons (n = 150) range from 0.11 - 3.91 mm in width and from 4.56 - 382.68 mm in length; although ribbon widths vary substantially, approximately 10 measurements per sample show ribbon width to be uniform through individual samples. The width of *Grypania* ribbons is generally less than 1.5 mm. Most specimens of *Grypania* with ribbon widths > 1.5 mm are from the Rohtas Formation in India; only a single specimen from the Greyson Shale in Montana has a ribbon width greater than 1.5 mm. *Grypania* ribbons are commonly less than 90 mm long and only 18 out of all specimens measured exceeded 90 mm in length. Coil diameters (n = 119) vary from 1.46 to 27.57 mm. Based on the total population of samples in this study (n = 152), *Grypania* specimens most commonly possess than less than 6 coils. Number of coils, however, combined with the very large difference in ribbon length, suggests that data reflects broken pieces of a larger organism.

Coiling patterns can be quantified with measurements of the area of the smallest and largest coils within a *Grypania* coil. Gathering data for the area of a circle best fit to the arc of the ribbon, the arc length for a given angle can be calculated by calculating the radius of that circle and fixing θ at 45°. The arc length of the smallest coil (s1) divided by the arc length of the largest coil (s2) yields a ratio (s1/s2) that can be used to quantify the degree of coiling for *Grypania* ribbons, where straight ribbons have s1/s2 values ~1 and intensely coiled *Grypania* specimens will have a ratio of ~0 (Fig. 14). The s1/s2 ratio of the population in this study suggests that *Grypania* favors coiling patterns between 0.3 and 0.7, suggesting that *Grypania* favors neither tight coils nor loose coils, or that there is moderate variability in coil tightness along the length of the ribbon. Coil diameters measured from *Grypania* specimens are more varied and no relationship is found between the degree of coiling and the number of coils preserved. Unlike the number of coils there does not appear to be a favored coil diameter favored, which may suggest that most of the coils preserved are incomplete organisms or that coil diameter is only loosely controlled by biology. The majority of specimens have coil diameters between 3 and 18 mm, consistent with previous reports of *Grypania* coil diameters (Walter et al., 1976; Walter et al., 1990; Han and Runnegar, 1992; Horodyski, 1993).

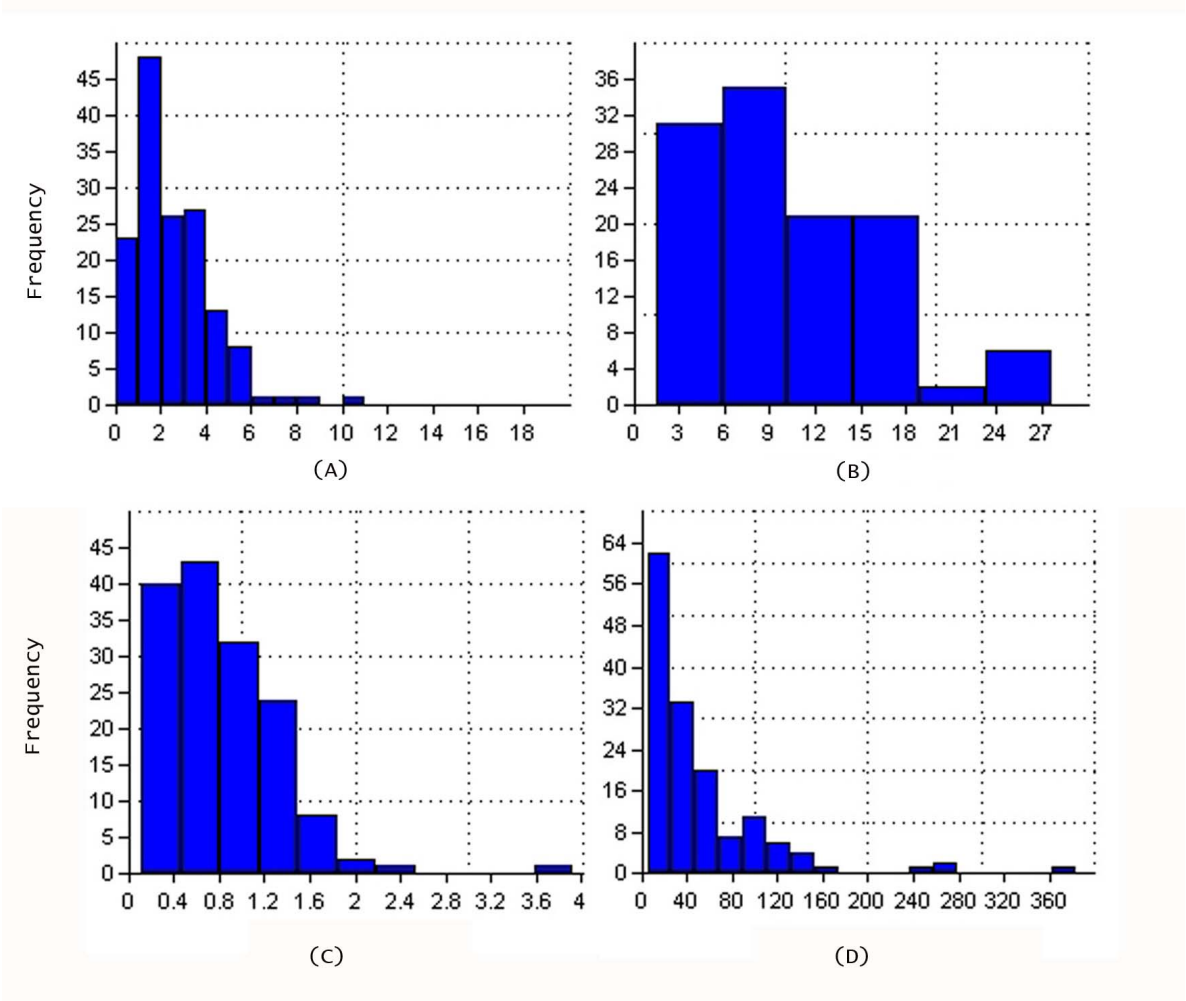


Fig. 13. Morphometric measurements of *Grypania* specimens. Frequency distributions of (a) number of coils, (b) coil diameter, (c) ribbon width, and (d) ribbon length of *Grypania* in this study (n=150). Bins were determined using the Zero Stage Rule of Wand (1997) in order to minimize binning artifacts. Measurements are recorded in millimeters.

Size frequency distributions are all positively skewed, which suggests either high rates of infant mortality or taphonomic conditions that would cause *Grypania* ribbons do disaggregate into smaller pieces (Hammer and Harper, 2006).

Once the preserved morphology of *Grypania* is known, the question then becomes how the preserved form relates to the original live form? To answer this question the morphological characteristics of *Grypania* coils, as measured from digital photographs, were used to model two conceptual possible body forms, each of which could be preserved as a flattened coil.

In the first model, G*rypania* is envisioned as a spherical planktic organism prone to uncoiling, similar to the peeling of an apple, after the organism's death (Fig. 14). Uncoiling of a spherical object would be expected to result in a planar coil represented by successive coils of greater diameter that increase in diameter via an arithmetic function (an Archimedean coil). In order to evaluate the size of organism that would potentially result in such a coil, ribbon width and length were used to calculate an area, which was then be equated to the surface area of a spherical organism of radius r ($A = 4\pi r^2$). The calculated radii were then used to determine the volume of a spherical *Grypania* organisms by $V = (4/3)\pi r^3$. Surface area-to-volume ratios were calculated for *Grypania* and compared to Precambrian macroalgae (Xiao and Dong, 2006).

A more common reconstruction of *Grypania* is as a simple compression of a coiled or helically coiled cylinder growing attached to the substrate (Fig. 15; Walter et al., 1990). Using the measured ribbon width for half the diameter of the proposed and the measured ribbon length for the height of the cylinder the surface area can be calculated by $A = 2\pi r^2+2\pi rh$. The volume of a cylindrical form for *Grypania* can then be calculated by $V = \pi r^2 h$. Surface to volume ratios are an important physiological factor that controls the metabolic rate of modern macroalgae with greater amounts of carbon fixed per body mass per unit of time being higher with higher surface to volume ratios (Xiao and Dong, 2006). The surface to volume ratios for spherical (max. 13 mm^2/mm^3) and cylindrical (max. 28 mm^2/mm^3) forms (Fig. 16) broadly agree with prior values determined for Mesoproterozoic carbonaceous compressions (max. 28mm^2/mm^3; Xiao and Dong, 2006). The agreement between the surface area to volume ratio of spherical and cylindrical forms for *Grypania* with other Mesoproterozoic carbonaceous compressions suggests that either of these morphological interpretations are plausible.

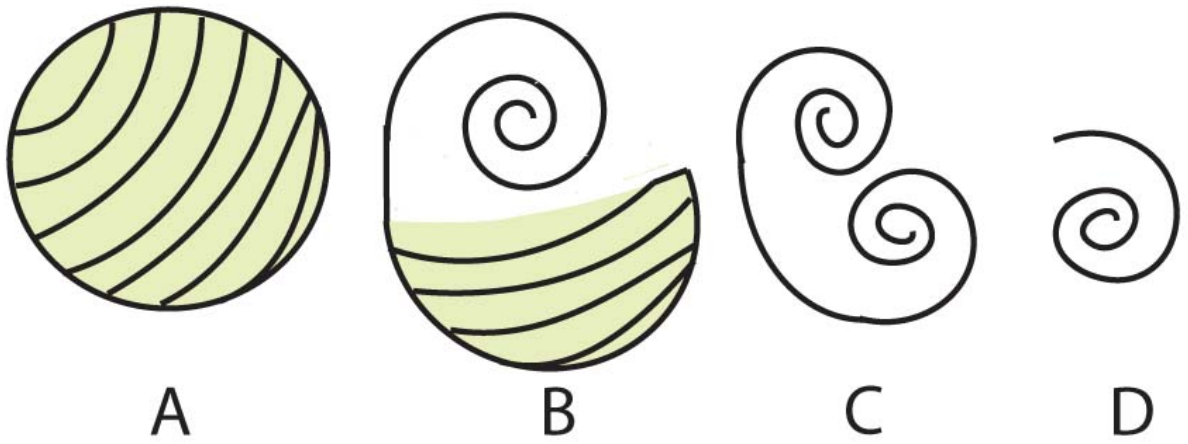


Fig. 14. Conceptual model for a spheroidal *Grypania* organism. A spheroidal, planktic *Grypania* (a) could plausibly decompose upon the organism's death by disaggregating along points of structural weakness (b). This taphonomic alteration of the original form plausibly produces the doubly-terminated coiled forms preserved in the rock record (c), with breakage resulting in the most common spiral morphologies (d).

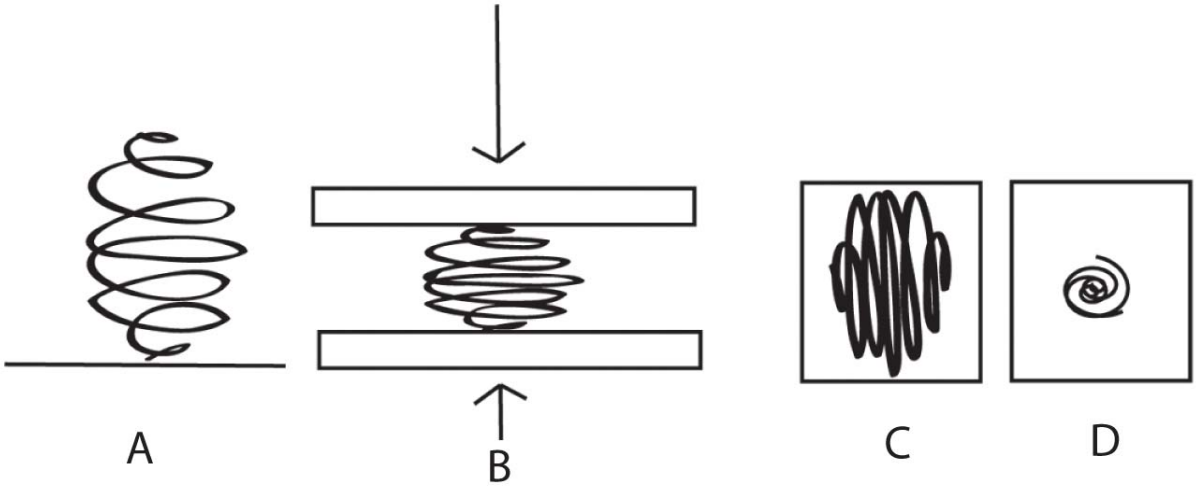


Fig. 15. Conceptual model for a helical *Grypania* organism. A benthic, ovoid helical form (a) can produce surficial markings by simple compression and burial (b), with variation in form resulting from rotation prior to compression (c), and taphonomic breakage of the organism (d).

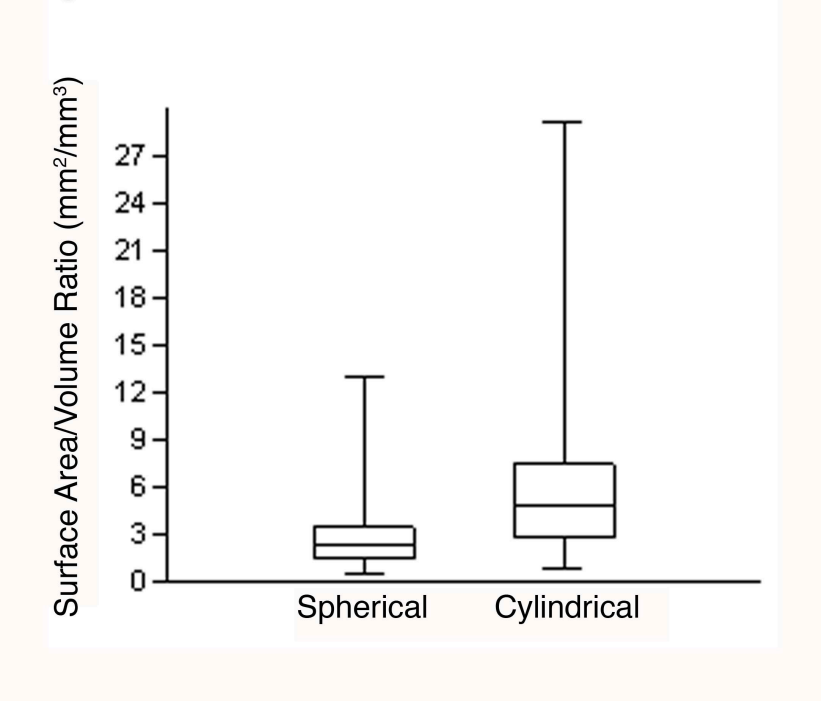


Fig. 16. Surface area-to-volume ratio for modeled spherical and cylindrical *Grypania* morphologies. The surface area-to-volume ratio (in mm^2/mm^3) is an important physiological trait that is well correlated to metabolic rates of modern macroalgae. Ratios calculated for *Grypania* agree with ratios estimated for other Mesoproterozoic macroalgae reported by Xiao and Dong (2006). Box and whisker plots show the median, upper and lower quartiles, and maximum and minimum values.

4.1.2 Morphological Interpretation

The preserved width of *Grypania* ribbons is the only morphological feature that is consistent within single ribbons throughout the study population; ribbon length, coil diameter, and the degree of coiling all vary. The quality of *Grypania* preservation varies with differences noted between part and counterpart of *Grypania* specimens as well as increasing grain size. Retention of the spiral shape and rare instances of folding indicate that the original organic material preserved was robust.

Despite morphological evidence supporting a spherical reconstruction for *Grypania* (i.e. rare doubly coiled specimens) the calculated radii of spherical *Grypania* are larger than known organisms and there are no modern organisms that are known to show taphonomic unwinding. Rather, the range of spiral morphologies of *Grypania* (e.g., increasing spiral diameter, overlapping coiling, doubly-terminated and single coils) suggest that an ovoid helical structure is

the morphologically most consistent reconstruction for *Grypania*; Fig. 15). A helical ovoid, rather than a true helix or cylindrical helix, best explains the variation in morphology of *Grypania* ribbons as they are preserved on the bedding plane. Bulbous features found at the end of some *Grypania* ribbons may represent holdfast structures. The rarity of potential holdfast structures may reflect depositional conditions wherein benthic *Grypania* was ripped from holdfasts during high energy events prior to deposition and burial. The role of taphonomy in *Grypania* preservation is likely significant. Unobscured ends of *Grypania* ribbons observed appear broken suggesting that the fossil material is often not complete. The inconsistent coil diameter, ribbon length, and coiling patterns observed in the study population may be explained through breaking of the original helical structure, consistent with a high-energy depositional model.

Potential sheaths observed on *Grypania* ribbons in this study are unlike the specimen from the Rohtas Formation previously described as having a robust outer sheath and a slightly collapsed cellular trichome (Fig. 4 in Butterfield, 2009). The virtual absence of evidence for sheaths among *Grypania* specimens in this study and the robustness of sheath material in general suggests that "sheaths" observed in *Grypania* ribbons more likely result from concentrations of organic matter at the ribbon edges and vary due to taphonomic variation. Additionally, preserved ribbon edges may also represent *Grypania* sheaths, as sheaths are frequently the only morphological feature preserved within cyanobacteria (Bartley, 1996).

The division of *Grypania* into two genera, *Grypania* and *Katnia*, based on the presence or absence of annulations (Sharma and Shukla, 2009) does not account for taphonomic variation among specimens. The annulations observed within *Katnia* specimens described and depicted by Sharma and Shukla vary from distinct (Fig. 6 A-F in Sharma and Shukla, 2009) to indistinct septae (Fig 6G-J in Sharma and Shukla, 2009). These indistinct annulations appear to be .taphonomic and are very similar to the pattern produced by the differential preservation of *Grypania* specimens from part to counterpart. As shale is split to reveal carbonaceous fossils on the different bedding planes there are often differences in preservation for each part and counterpart of the shale due to the vertical position of the plane of splitting relative to the fossil material (Orr et al., 2009). Clearly annulated specimens of *Grypania* (Fig. 10a in the current study and Fig. 6a-6e in Sharma and Shukla, 2009) may represent a distinct *Katnii* genus, rather

than *Grypania*, where the annulations are cellular in origin. There are no specimens of *Katnii* observed from the Greyson Shale or the Gaoyuzhuang Formation. The lack of distinctly annulated specimens in the other Mesoproterozoic localities likely results from cellular dissemination or lysing of cellular contents, which resulted in the preservation of a non-annulated form described as *Grypania*.

4.2 Mode of Preservation

4.2.1 Environmental Scanning Electron Microscopy Secondary Electron Mode (ESEM-SED)

Grypania from the Greyson Shale, Gaoyuzhuang Formation, Rohtas Formation, and Negaunee Iron Formation were analyzed via ESEM-SED. Only 30 of the 75 specimens analyzed were visible in ESEM-SED mode. When visible, *Grypania* ribbons occur as slight topographic differences between the ribbon and surrounding shale matrix. These impressions occur primarily as a slight difference in surface relief, and a flattening, or smoothing, of the shale matrix (Fig. 17). One specimen of *Grypania* from the Rohtas Formation occurs adjacent to a calcite vein within the rock. In this specimen, the *Grypania* coil appears as a flattened impression into the shale surface and the vein appears as a distinct line of positive relief across the sample surface (Fig. 18).

Most other visible features of *Grypania* do not appear as topographic features in ESEM-SED mode under the operating conditions and excitation volumes used in this study (Fig. 19a through 19c). In particular, annulated specimens of *Grypania* rarely show clear topographic features in ESEM-SED, although a single example appears to have topographic variability with the same spacing and regularity of the annulations seen with light microscopy (Fig. 19).

Surficial markings of varying morphology that associated both with *Grypania* fossils and the *Grypania*-bearing rocks appear as stringy, spotted, and amorphous stains on bedding planes. These films are similar in both color and reflectivity to *Grypania* fossils when observed by reflected light microscopy. In ESEM-SED mode these films are similar to *Grypania* fossils and occasionally appear as shallow impression in the shale matrix, or a flattening or smoothing of the shale surface. Surficial markings found in association with Gaoyuzhuang *Grypania* are observed as a stippled impression when observed in SED mode that is rougher than the surrounding shale

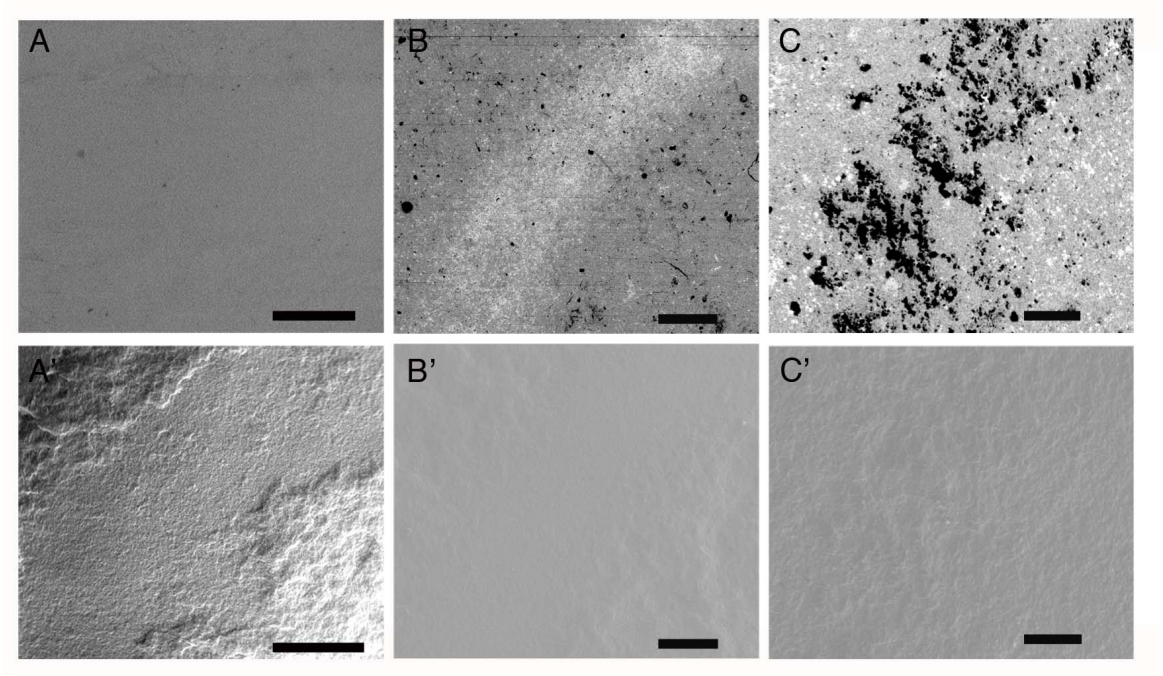


Fig. 17. ESEM images of *Grypania* ribbons in SED and BSD modes. *Grypania* ribbons are commonly not observed in BSD mode (a; sample GS-F23), but can be observed in SED mode as slight impressions in the shale matrix (a' and b'). Rarely, *Grypania* ribbons are observed as concentrations of bright spots that indicate the presence of elements with a higher average atomic mass than the surrounding shale matrix (b; sample GS-PCL). A single specimen of freshly split *Grypania* bearing shale reveals a lower average atomic mass in BSD mode (c; sample GS-F30) that suggests the possibility of organic material within the *Grypania* ribbon; this ribbon is not observed in SED mode (c'). Scale bars are 1 mm in (a) and 500 μm in (b) and (c).

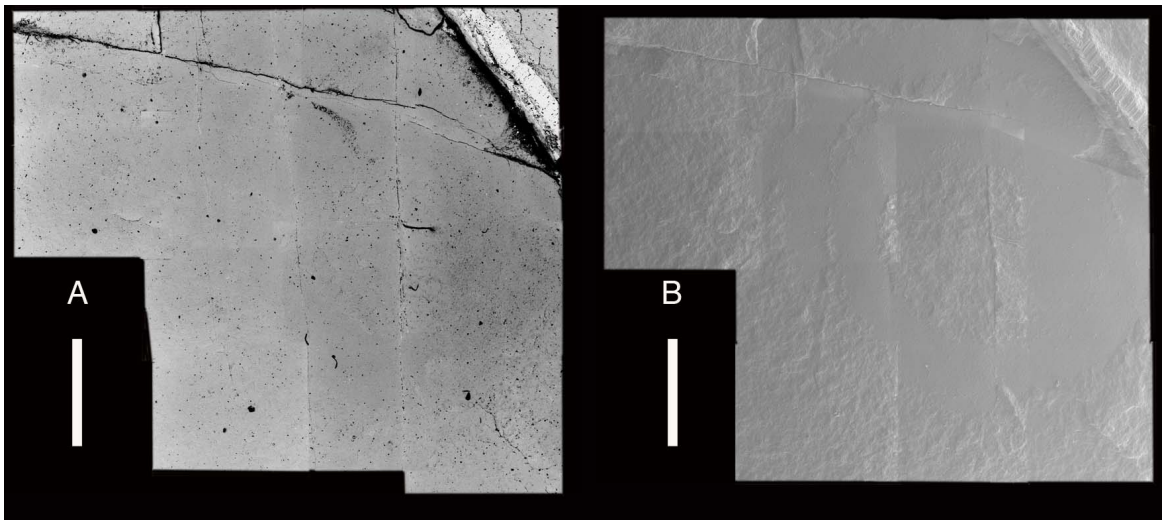


Fig. 18. Composite image of a *Grypania* coil adjacent to calcite vein. The ribbon in sample IND-C is not detected in BSD mode (a), however flattening of the shale is revealed when viewed in SED mode (b). Scale bars are 2 mm.

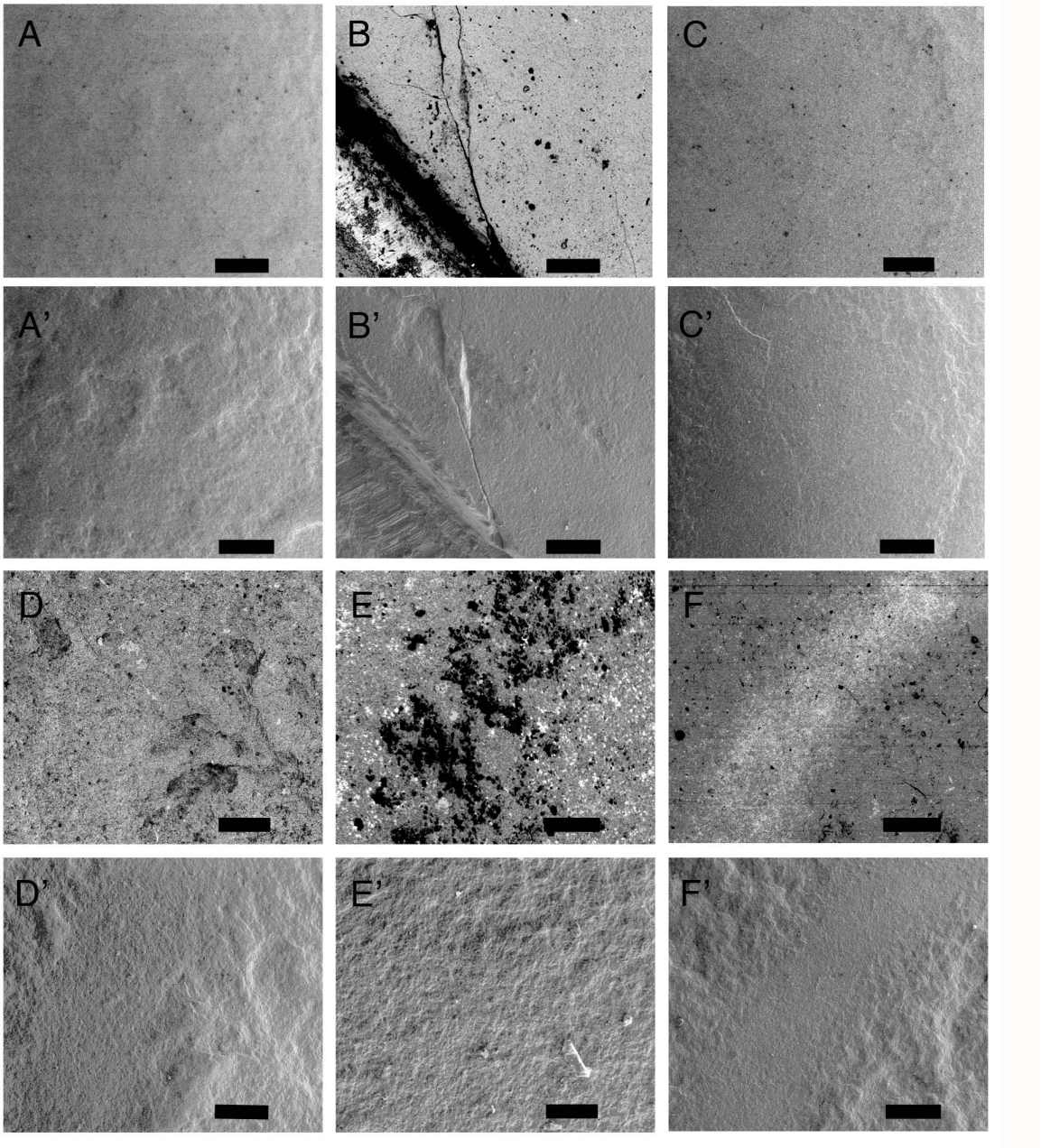


Fig. 19. ESEM images of annulated specimens of *Grypania* depicted in Figure 9. In rare instances, annulations appear as distinct topographic variations (a and a'); more commonly, no change in topographic expression is observed (b and b', c and c', d and d'). Occasionally, *Grypania* specimens are observed as concentrations of elements of relatively lower (e and e') or higher (f and f') atomic mass. Scale bars are 500 μm in (a), (b), (d), and (f); 1 mm in (b); and 200 μm in (e).

matrix. No films were observed in *Grypania* specimens from the Rohtas Formation or the Negaunee Iron Formation.

4.2.2 Environmental Scanning Electron Microscopy Backscatter Detection Mode (ESEM-BSD)

Most of *Grypania* ribbons analyzed with ESEM-BSD were not visible, and even those observed as a topographic impression in ESEM-SED mode were not detected in BSD mode. Rare examples of compositional differences were observed as either brighter areas (heavier average atomic mass) or darker areas (lighter average atomic mass) within the rock matrix. Concentrations of heavier elements were occasionally found within the *Grypania* ribbon, with a single specimen containing a concentration much greater than the surrounding shale (Fig. 17b). When brighter concentrations are viewed at high magnifications (~4000x) they reveal clusters of cubic to framboidal minerals, suggesting pyrite mineralogies (Fig. 20). Similarly, part of a single *Grypania* ribbon from a freshly split piece of *Grypania* bearing shale appears in ESEM-BSD mode darker color than surrounding shale matrix (Fig. 17c), which suggests the presence of preserved organic carbon.

The number of *Grypania* specimens available for analysis from the Gaoyuzhuang Formation, the Rohtas Formation, and the Negaunee Iron Formation were limited. *Grypania* from the Gaoyuzhuang Formation was detected with ESEM-BSD mode in a single specimen as a concentration of bright minerals within the ribbon that were not found in the surrounding rock matrix. Even the most distinctly annulated specimen from the Rohtas Formation does not contain any compositional difference between the ribbon and rock matrix. *Grypania* from the Negaunee Iron Formation was not readily recognized in ESEM-BSD mode, although framboidal pyrite does occur throughout the rock matrix. Other surficial markings observed with ESEM-BSD contained a similar range of morphologies, with higher concentration of the heavier elements within films relative to the surrounding shale matrix (Fig. 21).

4.2.3 X-Ray Energy Dispersive Analysis (EDS)

Most elemental maps produced for *Grypania* samples by X-ray energy dispersive analysis (EDS) did not reveal elemental differences between the *Grypania* ribbon and the surrounding shale, consistent with qualitative observations using backscatter detection (Fig. 22).

A few chemical differences are observed with EDS, specifically areas that appeared brighter in ESEM-BSD mode appear to have a distinct increase in Fe associated with them relative to bulk rock concentrations. Areas that appeared darker in ESEM-BSD have a distinct increase in C associated with them relative to bulk rock concentrations.

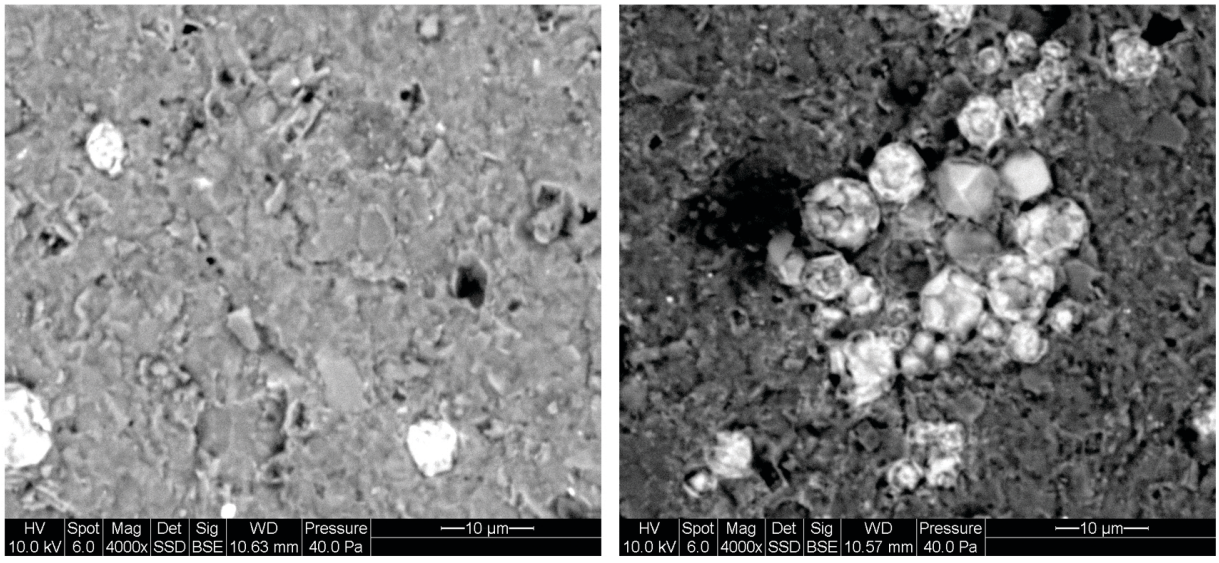


Fig. 20. Backscatter electron images of bright spots found within the matrix of *Grypania* bearing shale, sample BS-C. The bright spots appear to be crystals of framboidal pyrite. Scale bars are 10 µm.

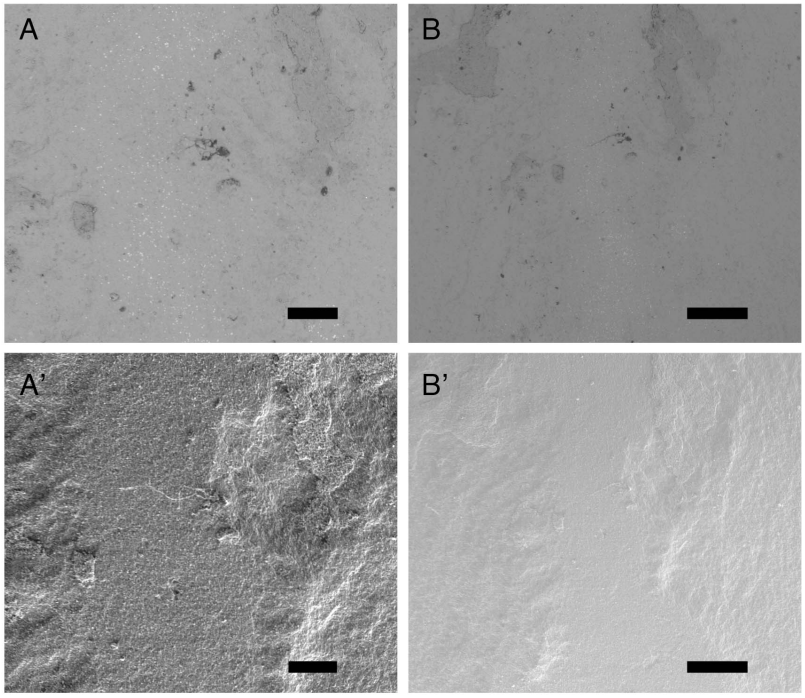


Fig. 21. ESEM analysis of surficial markings in *Grypania*-bearing shale. Chemical differences are observed in BSD as a concentration of pyrite within some surficial markings (a, sample GS-S27 and b, another view of GS-S27). Regions containing markings in these same samples also appear smooth compared to the surrounding rock matrix when viewed in SED mode (a' and b'). Scale bars are 500 μm in (a and a') and 200 μm in (b and b').

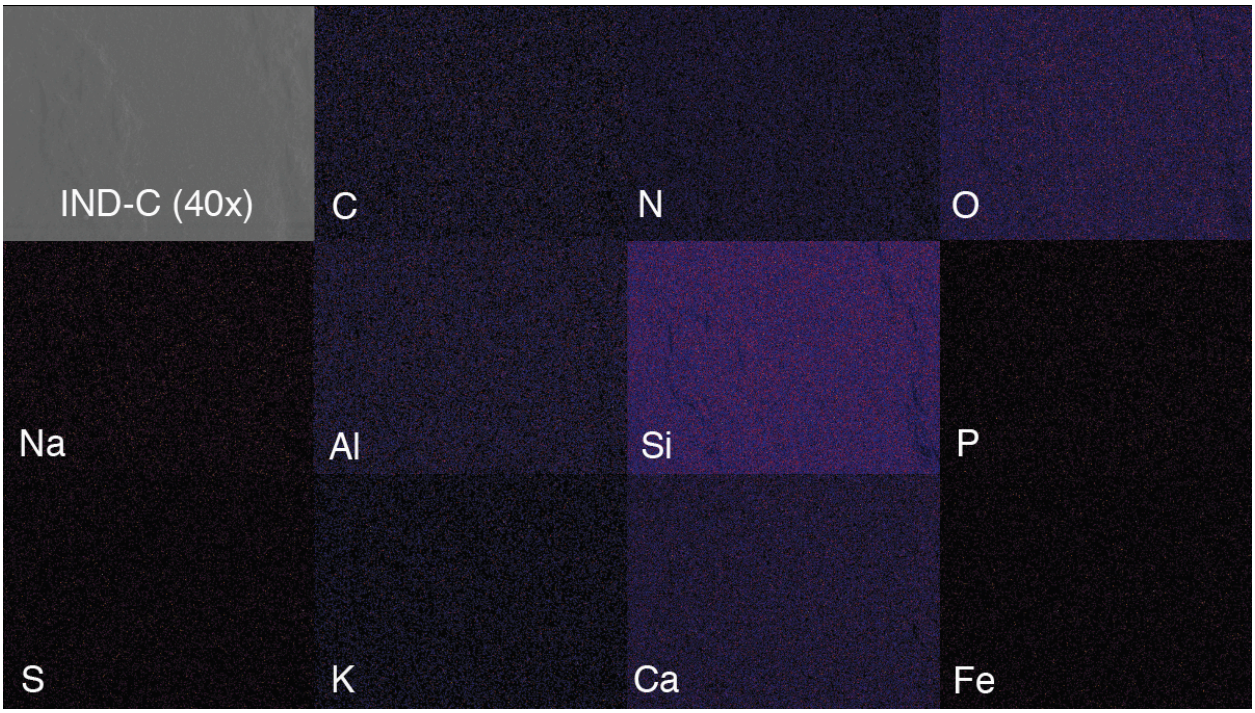


Fig. 22. ESEM-EDS analysis of *Grypania* ribbons. *Grypania* ribbons are typically not observed via elemental mapping of the *Grypania* ribbon relative to the surrounding shale matrix.

The few elemental maps that demonstrate an elemental difference between *Grypania* and the surrounding rock show an increase in the concentration of Fe along with a corresponding decrease in the concentration of Si (Fig. 23). EDS spectra gathered for these bright spots suggest that two mineralogies are present, an iron sulfide and an iron oxide. Absence of a sulfur signature in EDS mode may suggest necessity for longer count times. Other than the rare elemental signature for Fe detected with EDS, only a single specimen of freshly split *Grypania* from the Greyson Shale contained higher concentrations of C within the ribbon, which corresponded with a slightly lower Si content (Fig. 24). Annulations associated with this specimen are revealed in EDS mode to be composed of differential concentration of preserved carbon. These patches of carbon, however, are poorly defined and are likely to be preservational in origin, rather than biological.

Surficial markings associated with *Grypania*-bearing shale from the Greyson Shale and the Gaoyuzhuang formation were also mapped with EDS. Most markings did not reveal a compositional difference between markings and surrounding matrix. Several specimens, however, contained higher Si content and lower Al and K increases within surficial markings. Others, that appear as distinct impressions within the shale surface contained an increases in Fe and Ca and a decrease in Si associated with the film. The surficial film found of one sample from the Gaoyuzhuang Formation appears to have higher contents of C and Fe, with lower Si, K, and Mg abundance.

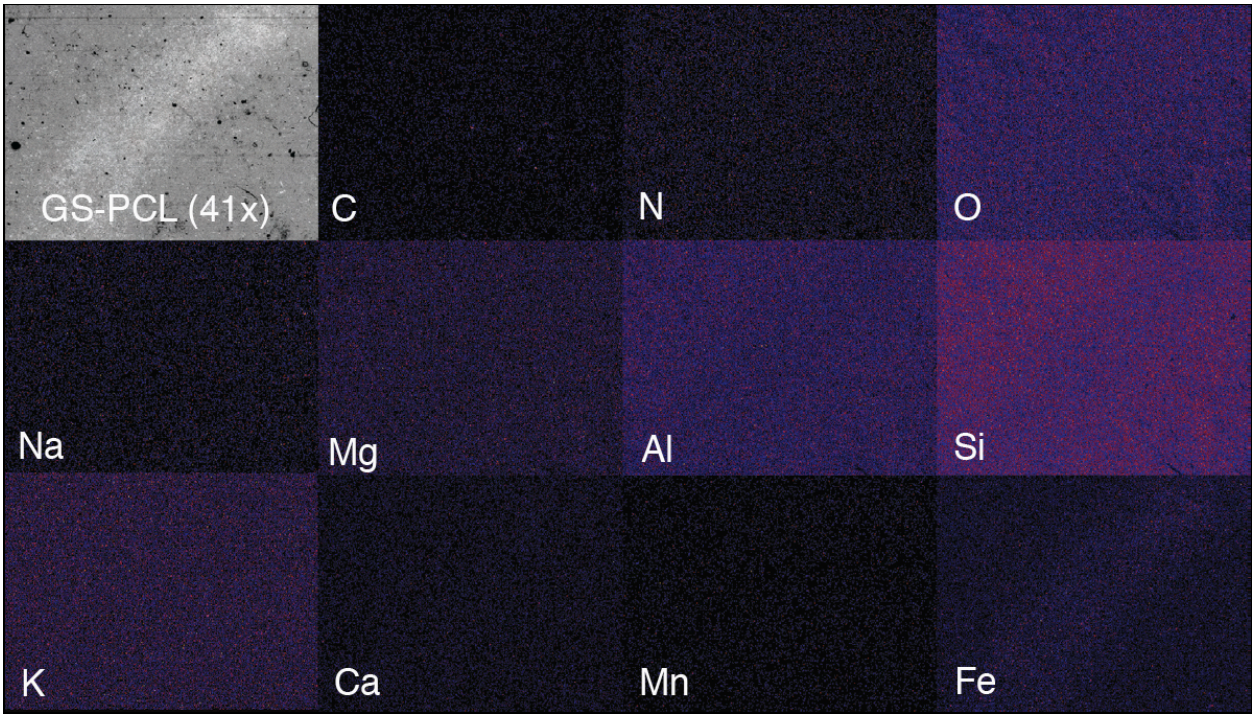


Fig. 23. *Grypania* ribbon observed in ESEM-EDS. In rare cases (e.g., sample GS-PCL) elemental mapping reveals and increase in the amount of Fe within the *Grypania* ribbon, which EDS spectra suggests results from pyrite and iron oxide mineralization.

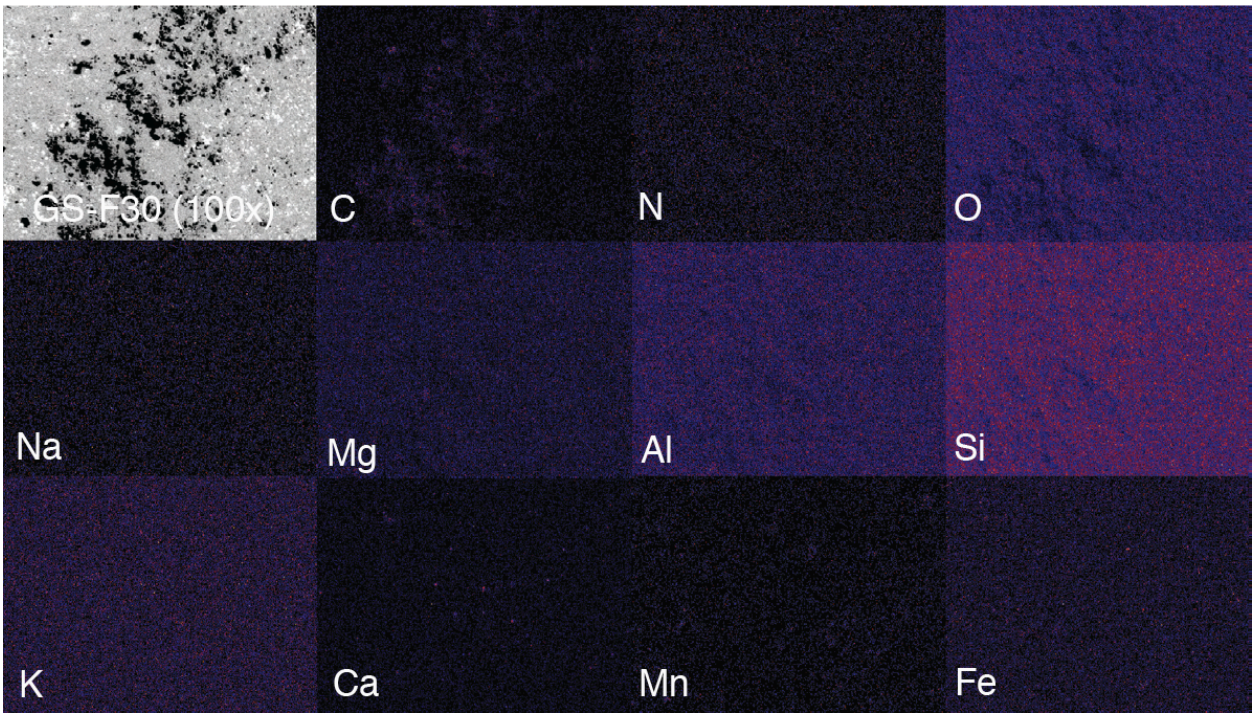


Fig. 24. *Grypania* ribbon observed in ESEM-EDS. A single specimen of freshly split *Grypania* (sample GS-F30) shows, via elemental mapping of this ribbon, a clear increase in the abundance of carbon within the ribbon relative to that in the surrounding shale matrix.

4.2.4 Interpretation of Preservation

Non-biomineralized tissues or "soft-parts" are prone to decay and thus are rarely preserved in the fossil record (Orr et al., 2002). In terms of Proterozoic macroalgae, however, preservation via compression is not uncommon, and only relatively few have been preserved by permineralization (Xiao and Dong, 2006). The use of organic preservation and carbonaceous compression to describe macroscopic "carbonaceous" organisms with minimal relief disguises the complexity of diagenetic processes involved in the preservation of non-biomineralized fossils (Orr et al., 2002). Additionally, *Grypania* and other macroscopic forms may be preserved as casts and molds similarly to Ediacaran organism (Droser et al., 2004). Most commonly, "carbonaceous" impressions (e.g. *Chuaria*) contain the most information in the preserved organic matter (Dutta et al., 2006).

In sharp contrast to the robust organic remains preserved in carbonaceous fossils such as *Chuaria*, ESEM imaging of *Grypania*-bearing rock reveals ribbon impressions, but show little unambiguous evidence for organic remains. *Grypania* ribbons were detected as impressions on 30 specimens from 78 gathered for ESEM analysis from the Greyson Shale, the Gaoyuzhuang Formation, and the Rohtas Formation. Ribbons observed with secondary electron imaging commonly appear as topographic depression, flattening, or smoothing of the mineral matrix. This surface flattening indicates that an object with physical properties contrasting with the muddy matrix was indeed present on the substrate prior to burial and was able to differentially compress, or reorganize, grains of the underlying substrate. This grain reorganization resulted in an increased level of grain packing prior to lithification. Evidence of this flattening is found in both part and counterpart of samples, indicating survival of material into at least the earliest stages of burial and compaction.

Grypania bearing shales show little evidence of compositional differences between the ribbons and the surrounding matrix. Only a single sample of freshly split Greyson Shale revealed a measureable increase in carbon within the *Grypania* ribbon relative to the surrounding shale matrix. This observation suggests that organic remains of *Grypania* are not prone to organic preservation. Only rarely preserved organic signatures suggest that *Grypania* may have consisted primarily of thin, easily oxidized organic films, or that the majority of organic material in *Grypania* was destroyed by diagenetic processes.

The more common chemical difference identified in *Grypania* are higher concentrations of elements in the region of the ribbons that are of higher atomic mass than the surrounding matrix. These heavier elements have framboidal or cubic structures when viewed at high magnifications and elemental spectra indicate the presence of two mineralogies, an iron sulfide interpreted as pyrite and an iron oxide interpreted as goethite, hematite, or magnetite Increased concentration of pyrite within *Grypania* ribbons likely reflects organic carbon oxidation, via either microbial sulfate reduction or iron reduction during early diagenesis (Canfield et al., 1993). Early diagenetic deposition of pyrite is common in normal to suboxic marine sediments (Canfield et al., 1993; Tribovillard and Lyons, 2008) and has been shown to be a primary mechanisms of fossil preservation in some soft-bodied lagerstätten (e.g. Wheeler Shale, Vorhies and Gaines, 2005; Hunsruck Shale, Briggs and Bartels, 2010). Furthermore, because pyrite is not prone to later diagenesis (Taylor and Curtis, 1995), the relatively low concentrations of pyrite observed in *Grypania* samples suggests initially low carbon contents for *Grypania*.

The vast majority of samples analyzed via ESEM-BSD and ESEM-EDS, showed no geochemical signature for *Grypania* ribbons above the background rock matrix. Absence of distinct geochemical signatures within *Grypania* ribbons suggest that original organic preservation, clay templating, iron reduction and iron sulfide precipitation, or manganese reduction (Butterfield, 1990; Vorhies and Gaines, 2005; Briggs and Bartels, 2010) was minimal, and supports the hypothesis that *Grypania* organic matter may never have been abundant and was not likely to have survived long past original burial. In low oxygen Mesoproterozoic ocean (Kah et al., 2001; Luepke and Lyons, 2001; Kah et al., 2004; Gellately and Lyons, 2005), microbial remineralization of organic carbon would have occurred soon after burial. Stability of mineralogical byproducts would be expected to survive even greenshist-stage maturation (Gaines et al., 2006). Similarly, clay templating of organic material is often associated with nonmineralizing organisms during burial (Butterfield, 1990). That pervasive templating did not occur during burial and through metamorphism of the Greyson Shale, suggests that little, if any, organic matter survived to this stage. All these observations suggest that *Grypania* fossils may represent organic-poor sheathes only a new micrometers in thickness; in this case, it is entirely plausible that the bedding plane expression of *Grypania* may, in fact, preserve organic material

which has been rendered invisible by SEM detection limits via beam interaction with the shale matrix.

Although the potential exists for *Grypania* to consists of thin organic films undetectable by SEM, the paucity of morphological features and the near absence of mineralogical differences between the ribbons and matrix suggest taphonomic processes have largely destroyed the original organic structure. The following scenario is presented as one possible model for the deposition and preservation of *Grypania*. In this scenario, rooted benthic ovoid helical *Grypania* were likely broken from the original growth position during storm or tidal events that transported the material for immediate burial. Flexibility of the original organism in the translational plane of the helix can explain the range of variation observed for *Grypania* ribbons. Autochthonous *Grypania* deposited upright may result in the overlapping spiral pattern produced by flattening of the original ovoid helix, and allochthonous organisms may be deposited skewed from the upright position resulting in lopsided or un-spiraled *Grypania* (Fig. 25). Transport conditions prior to fossil preservation may thus strongly affect the preservation of the organism prior to burial; the likelihood of preserving a full specimen is extremely low. Water turbulence could act as the breaking stress for the organism as it is transported or ripped up. Smaller pieces of *Grypania* would be preserved as the incomplete specimens with the various morphologies observed.

Additionally, decomposition may have strongly affected preservation. Decomposition reactions facilitate the precipitation of minerals (i.e. pyrite) on decaying tissues replicating their structure (Briggs, 2005). These minerals generally have a greater chance of being incorporated into the fossil record than the original unaltered organic remains (Gaines et al., 2008). Another common mode of fossil preservation for carbonaceous material is tissue replication by clay minerals within the early burial environment (Orr et al., 1998). While authigenic mineralization of organic matter is commonly associated with carbonaceous fossils, preservation with no compositional differences detected between the fossil material and rock matrix is also found (Gaines et al., 2008). Fossils without distinct compositional differences commonly contain degraded carbon films, which are sufficient enough to define the morphological features of the specimen, but do not retain sufficient carbon to be reliably detected (Gaines et al., 2008).

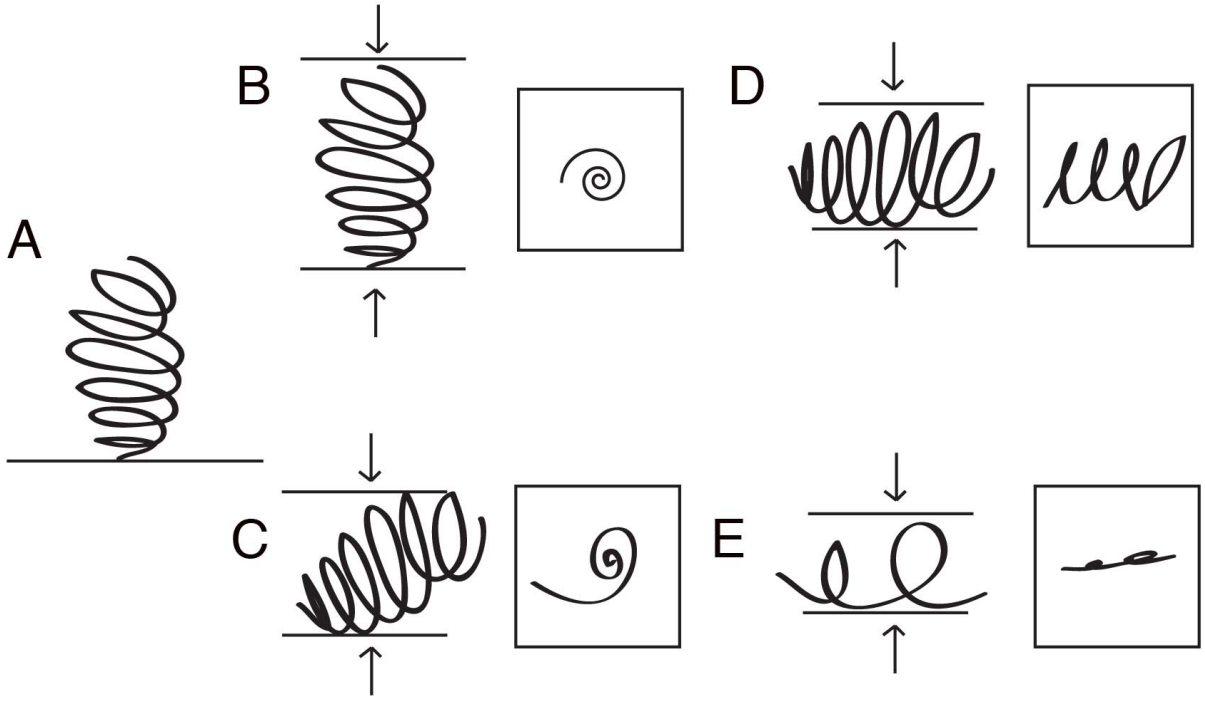


Fig. 25. Possible depositional model for *Grypania*, which can explain some of the variation observed for *Grypania* coiling patterns. The original helical coil can be compressed in a variety of ways to result in the impressional features preserved on the bedding planes of these Proterozoic shales.

4.3 Ultrastructure of Grypania

Analysis of acid macerations of Greyson Shale samples yielded no recognizable microfossils. Additionally, no macroscopic portions of *Grypania* were recovered from the macerations. Analysis of polished thin sections perpendicular to the bedding plane with SEM-EDS at Oak Ridge National Laboratory do not indicate a concentration of organic matter or diagenetically altered organic matter at the surface or below the bedding plane where *Grypania* is located. Ribbon impressions are observed in the polished thin sections (Fig. 26). These impressions or indentations are slight, typically ~340 μm deep, along the bedding plane.

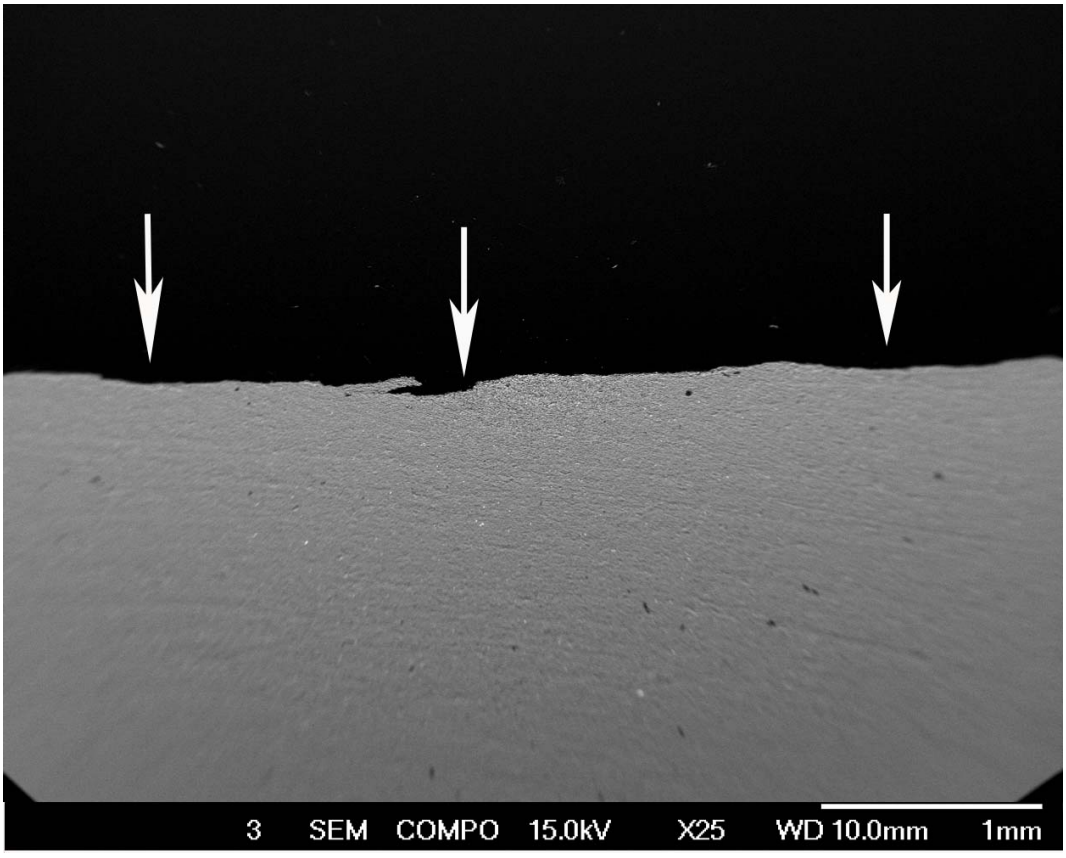


Fig. 26. *Grypania* ribbons indentified as impressions in thin section perpendicular to the bedding plane that are approximately 340 μm deep. Arrows indicate the location of the impression. Scale bar = 1mm.

4.3.1 Ultrastructural Interpretation

Acritarchs, believed to be the remains of unicellular, eukaryotic algae (Traverse, 2008), are common in Mesoproterozoic successions. The current attempt at acid maceration of *Grypania* bearing shale for microfossils was consistent with prior attempts, with no macro or microscopic organic remains recovered from either the Gaoyuzhuang Formation or Rohtas Formation (Walter et al., 1990; Kumar, 1995; Sharma and Shukla, 2009). Consistent with ESEM, SEM, and EDS observations of *Grypania* there appear to be no clear preservation of organic walls associated with *Grypania* fossils. Acritarchs, interpreted as eukaryotic algae, are found elsewhere within the Belt Supergroup stratigraphically above the Greyson Shale within the Libby Formation (~900-10000 Ma; Kidder and Awramik, 1990). Additionally acritarchs are found within Proterozoic rocks form Asia in the Chuanlinggou Formation in China (~1700 ma) and the Tirohan Limestone in India (~1600 Ma) though each acritarch taxa recovered lacks indisputable evidence supporting a eukaryotic affinity (Peng et al., 2009). The presence of Acritarchs in formations associated with *Grypania*-bearing localities that have undergone similar diagenetic histories suggests that there is likely an absence of eukaryotic organisms within *Grypania*-bearing environments. This can imply that environmental factors may have inhibited algal growth, supporting a bacterial origin for *Grypania*.

4.4 Biochemistry of Grypania

4.4.1 Coulometry

The organic carbon content measured from the Greyson Shale range from 0.20 to 0.38%. No significant variation in organic content is noted through the shale, although there is some indication of variability in carbonate content, most likely associated with carbonate-filled cracks and joints that occur in the unit (Table 3). XRD analysis of the Greyson Shale show approximately 20% quartz, 12% muscovite/illite, 12% chlorite, 6% albite, 3% calcite, and 3% dolomite, with the rest of the rock characterized as X-ray amorphous. There is also no indication of greater concentrations of organic carbon within unweathered shale collected at ~ 0.75 m depth (0.23 - 0.34% C_{org}) vs. more highly weathered surface samples (0.19 - 0.30% C_{org}). Selected pieces of *Grypania* ribbons, isolated as much as possible from the bulk matrix, were also compared to the bulk rock for weathered *Grypania* ribbons. The values recorded for the organic

carbon content of these samples do not differ from the bulk rock, supporting earlier observations that *Grypania* ribbons do not contain substantial organic carbon. Organic carbon values associated with the *Grypania* from the Gaoyuzhuang Formation (0.34 and 0.26% C_{org}) are marginally higher than the values recorded from the bulk matrix (0.16 and 0.26% C_{org}, respectively), suggesting that the Gaoyuzhuang Formation might present a better target for detailed analysis of organic matter associated with *Grypania*.

Table 3

Carbon concentrations recorded in *Grypania*-bearing shale.

Sample*	C_{tot} (wt %)	C_{carb} (wt %)	C_{org} (wt %)
GS-1	0.30	0.10	0.20
GS-2	1.72	1.38	0.34
GS-3	0.20	0.00	0.20
GS-4	0.22	0.01	0.21
GS-5	0.42	0.04	0.38
GS-6	0.36	0.03	0.33
GS-7	0.31	0.00	0.31
FR-2	0.92	0.58	0.34
FR-5	0.86	0.60	0.26
FR-7	0.64	0.41	0.23
FR-9	0.56	0.33	0.23
W-1	0.87	0.65	0.22
W-3	0.52	0.22	0.30
W-5	0.96	0.65	0.31
WG-1	0.27	0.00	0.27
WG-3	0.32	0.00	0.32
WG-5	0.22	0.03	0.19
WM-1	0.23	0.00	0.23
WM-3	0.19	0.00	0.19
WM-5	0.60	0.33	0.27
GAO-G1	0.34	0.00	0.34
GAO-M1	0.26	0.00	0.26
GAO-G3	0.21	0.00	0.21
GAO-M3	0.16	0.00	0.16

* FR denotes fresh sample; W denotes weathered sample; WG denotes *Grypania* isolated from weathered samples; WM denotes weathered matrix containing no visible *Grypania*.

5. Discussion

5.1 Biological Affinity of Grypania

In the absence of clear morphological, ultrastructural, or geochemical evidence m understanding the taphonomic history of *Grypania* is important for determining its biological affinity. Taphonomy can affect both the morphological characteristics and chemical composition of organic material commonly used to discriminate fossil material (Bartley, 1996). Any original organic material preserved for these compression fossils has been subjected to decomposition, diagenesis, burial, and low-grade metamorphism. Although rare, the presence of ribbon folding and breakage within *Grypania* ribbons demonstrates that *Grypania* existed as discrete bodies during sedimentation (Walter et al., 1976). The robustness of the original cellular material relative to unlithified muddy matrix is supported by observations of distinct impressions of *Grypania* ribbons with ESEM-SED. Occasional concentrations of carbon and diagenetic pyrite identified with ESEM-BSD and ESEM-EDS found within *Grypania* ribbons also suggest that organic material was present within the ribbons for at least a short time after burial.

The true affinity of *Grypania*, however, is more difficult to discern. Raymond (1935) suggested that it was not improbable for macroscopic carbonaceous compressions to be algal in origin. Ribosomal RNA molecular phylogeny and the recovery of steranes place the divergence of eukaryotic organisms early in Earth history (~2.7 Ga) making a eukaryotic interpretation for *Grypania* plausible (Woese et al., 1990; Javaux et al., 2003; Knoll et al., 2006). Also, with the exception of *Grypania* from the Negaunee Iron Formation (~1.9 Ga), most *Grypania* occurrences are in the Mesoproterozoic, by which time both eukaryotic organisms (Javaux et al., 2004) and multicellularity (Grey and Williams, 1994; Butterfield, 2000) were well established. The appearance of *Grypania* as a macroscopic form at 1.9 Ga has thus been used as a marker for body size increase in the Paleoproterozoic with a pronounced jump in body size (~6 orders of magnitude) thought to be driven by the emergence of the eukaryotic cell and multicellularity (Payne et al., 2009). Unfortunately, at present there is no direct evidence suggesting that *Grypania* is indeed eukaryotic.

The consistency of size within *Grypania* populations has been used as evidence for a eukaryotic affinity (Knoll, 1992; Knoll et al., 2006). The ribbon width is the only consistent

morphological characteristic observed within the 150 specimens measured, but although uniform within single ribbons, widths (0.1-1.7 mm) within the population varied by an order of magnitude. Large variations in ribbon length (4.5-383 mm) and coil morphology are observed (coil diameter, 0-21 mm; number of coils, from zero to 11 coils; and tightness of coils) for all specimens. Much of this variation may be attributable to taphonomic breakage of a larger organism so the true size range of *Grypania* is unknown.

Stronger evidence, perhaps, for a eukaryotic origin lies in the large size of *Grypania* and the potential of annulations in some specimens. The macroscopic size of *Grypania* coils has been also been used to advance a eukaryotic affinity for *Grypania* fossils (Walter et al., 1976, Walter et al., 1990; Knoll, 1992). The ribbon and coil size measured from *Grypania* fossils falls within the range of multicellular and eukaryotic algae that are generally considered macroalgae (>1mm; Xiao and Dong, 2006), although macrobacteria are known from oxygen deficient zones (Schulz et al., 1999; Schulz and Schulz, 2005). Most taxonomically resolved fossil and modern macroalgae are benthic, and evidence of broadening at *Grypania* ribbon ends further support a benthic habit for *Grypania*. Similarly, the presence of annulations on some specimens of *Grypania* has been used as evidence of a multicellular eukaryotic origin (Kumar, 1995). These annulations, however, provide only ambiguous evidence of multicellularity. In order to affirm a eukaryotic origin, these annulations must be shown to be true transverse septae (Samuelson and Butterfield, 2001). No samples from this study contain unambiguous septae, and most observed annulations are interpreted as taphonomic in origin. Furthermore, *Grypania* specimens with the most exquisite preservation (Figs. 4C,D and 6A,E in Sharma and Shukla, 2009) reveals individual cells within a single outer sheath, which more strongly supports interpretations of *Grypania* as multicellular or coenocytic filamentous bacteria (Samuelsson and Butterfield, 2001). Broader occurrence of annulated forms within the Rohtas Formation may reflect wither differential preservation, or perhaps true species division (Sharma and Shukla, 2009). Many specimens from this study and others (Figs. 4C,D and 6B,D in Sharma and Shukla, 2009) show only a vague indication of annulations, which plausibly reflect nothing more than a taphonomic variant caused by either wrinkling of the organism during burial, causing differential part/counterpart preservation, or possibly differential mineralization of cell walls during early diagenesis.

Acetabularia, a dasycladacean green alga that grows as a narrow cylinder about 0.4 mm in diameter with lengths up to 180 mm, has been proposed as the closest possible analogue for *Grypania* (Crawley, 1964; Han and Runnegar, 1992), however the preserved morphology of *Grypania* ribbons does not match either modern or fossil morphologies (LoDuca and Behringer, 2009). Knoll (1992), however, suggested that *Grypania*, if eukaryotic, might have belonged to an extinct algal group with no modern analogue.

No specimens of *Grypania* analyzed in the current study show clear differentiation of sheath and cellular material recognized in some exquisitely preserved specimens (Fig. 4 in Butterfield, 2009). Butterfield (2009) on the basis of this feature has interpreted as a simple coenocytic filament with a more or less undivided cytoplasm and morphological complexity similar to true multicellular organisms. The absence of clear cellular components found in association with *Grypania* fossils in this study also highlights the role of taphonomy in fossil preservation. Although sheath material is notoriously robust, some cyanobacteria have relatively thin sheaths (Bartley, 1996). The lack of distinctly preserved organic material, or indication of internal cells, for the majority of *Grypania* fossils may, in fact, support a bacterial affinity, wherein internal trichomes escaped during the burial process and a thin sheath, while robust enough to compact sediment substrate during initial burial was prone to early decomposition. Early decomposition and release of dissolved organic matter to the sediment pore space would also prevent substantial templating later in diagenesis, resulting in the vague, often diffuse stains observed for most *Grypania*.

Although coiling morphology is common for cyanobacterial groups (Sharma and Shukla, 2009), comparison of *Grypania* size ranges suggest that *Grypania* fossils are nearly 2 orders of magnitude larger than known bacteria and cyanobacteria that exhibit a coiled morphology (see also Vidal, 1989; Han and Runnegar, 1992; Sharma and Shukla, 2009). Cyanobacteria such as *Nostoc* and *Wollea*, however, are known to attain macroscopic size through the alignment of microscopic trichomes with a common tubular sheath have been suggested to be similar to *Grypania*, though these cyanobacteria are filamentous and wavy rather than coiled (Walter et al., 1990; Sharma and Shukla, 2009). And, although they lack the coiling morphology, sheath material of giant filamentous sulfur bacteria such as *Beggiatoa* and *Thioploca* are consistent with the size of *Grypania* (Han and Runnegar, 1992; Sharma and Shukla, 2009). Coiling morphology

may simply be an ambiguous characteristic in the argument for taxonomic affinity. Coiling in microorganisms is often associated with motility or light capture. For a proposed benthic *Grypania*, increasing coil size may simply provide increased light gathering ability in a turbid lagoon environment.

Although evidence for eukaryotic organisms remains ambiguous, neither a prokaryotic nor eukaryotic interpretation necessarily rejects the possibility of multicellularity. Multicellularity is not exclusive to eukaryotic organisms and is exhibited by cyanobacteria, green non-sulfur bacteria, large sulfur bacteria, and myxobacteria among others (Butterfield, 2009). Macroscopic size and potential annulations are the driving features of eukaryotic interpretations for *Grypania* (Walter et al., 1976; Walter et al., 1990; Han and Runnegar, 1992; Knoll, 1992; Horodyski, 1993; Kumar, 1995; Sharma and Shukla, 2009). The current study has failed to identify any structures that might be clearly interpreted as eukaryotic, including complex multicellular filaments with terminal differentiation, wall ultrastructure, processes extending from cell walls, excysement structures, wall ultrastructure, tissue differentiation, or well-defined wall chemistry (Javaux et al., 2003; Butterfield, 2009). Combined with the high degree of disaggregation, early diagenetic decomposition, and the lack of preserved cellular or sheath found within other eukaryotic Proterozoic fossils (Butterfield, 2000, Javaux et al., 2003; Sharma et al., 2009) features suggest a multicellular bacterial affinity for *Grypania*.

5.2 Environmental Implications of Grypania

The distinction between prokaryotic and eukaryotic affinities, regardless of multicellular habit, is critical in terms of our understanding of Precambrian environmental evolution. Multicellularity, in itself, carries large implications for biotic evolution, by establishing morphology as a significant factor in the evolutionary process (Butterfield, 2000). However, linkage of multicellularity to eukaryotic metabolisms has much more explicit environmental implications. Efforts to constrain the timeline of eukaryotic evolution using molecular dating techniques have suggested that there is a significant relationship between the complexity of life forms and the increase in oxygen levels through the Precambrian (Hedges et al., 2004). Anoxic conditions serve as an environmental barrier to the development and diversification of eukaryotic life, since eukaryotes require oxygen for the production of sterols (Runnegar, 1991; Schouten et

al., 1998; Javaux et al., 2004), although sterol production in low partial pressures of oxygen is possible and could be found localized oases of oxygen (Knoll, 2006). The molecular oxygen requirements of eukaryotes, and the appearance of *Grypania* as a possible multicellular eukaryotic alga has been used to independently suggest that atmospheric oxygen levels had risen to the minimum level required for aerobic respiration (Runnegar, 1991). Whereas such arguments may not necessarily place constraints on Belt Supergroup, Gaoyuzhuang Formation, Rohtas Formation *Grypania* (1.4-1.6 Ga) as multicellular eukaryotes, they pose a greater problem when Negaunee Iron Formation *Grypania* (1.9 Ga) is considered.

The history of biological evolution through the Proterozoic is critically constrained by ocean and atmospheric chemistry. The Great Oxidation Event (GOE; Holland, 2006), at approximately 2.2 Ga, represents the fundamental shift in the Earth's biosphere during which the Earth's atmosphere and oceans transitioned from dominantly reducing to dominantly oxidizing. The hallmark signature of the GOE is a 10‰ positive shift in the C-isotope composition of marine carbonates lasting ~100 to 160 Ma (Karhu and Holland, 1996). This positive shift in $\delta^{13}C$ is attributed to the increased burial of organic carbon leading to oxygen levels to greater than 2×10^{-3} (or 10-5 PAL; Farquhar and Wing, 2003; Bekker et al., 2004). Cyanobacterial production of oxygen is also universally believed to have attributed to the initial oxygen rise at 2.3 Ga, since cyanobacteria survive both anaerobically and aerobically (Holland, 1994; Farquhar et al., 2000; Kasting and Siefert, 2002). This shift in carbon isotopes occurs in concert with broad scale replacement of reduced detrital minerals, such as pyrite, with oxidized (i.e. hematitic) components (Holland, 1994).

Thus, at the time of the first appearance of *Grypania* (Han and Runnegar; 1992), the Earth's oceans would have been transitioning from oxic at the surface to anoxia and sulfidic at depth (Canfield 1998; Poulton et al., 2004). *Grypania* are problematic in that they may not be true *Grypania,* similar to those found within the Mesoproterozoic (Samuelsson and Butterfield, 2001), or they may have evolved within a transient oxygen high soon after the GOE (Bekker et al., 2004). Furthermore, large and systematic stratigraphic variation in $\delta^{34}S$ measured from carbonate associated sulfate (CAS) in the Mesoproterozoic (Kah et al., 2001; Kah et al., 2004; Gellatly and Lyons, 2005) as well as heavy and variable $\delta^{34}S$ of pyrite (Lyons et al., 2000; Shen et al., 2003) and a growing body of evidence from Fe speciation (Raiswell and Canfield, 1998)

and Mo isotopes (Lyons et al., 2009) that suggest low oxygen, potentially sulfidic conditions persisted well into the Neoproterozoic.

If marine systems remained anoxic and sulfidic below the surficial mixed layer through the Proterozoic, then both dissolved iron and molybdenum would have been limited. Dissolved iron and molybdenum are important components of the enzymes responsible for nitrogen fixation and assimilation indicating that nitrogen cycling in Mesoproterozoic oceans would have been scarce (Anbar and Knoll, 2002). Thus lower concentrations of Mo in the oceans would affect primary productivity as Mo is commonly used in nitrogenase for nitrogen assimilation forcing organisms to use the less efficient Fe nitrogenase (Anbar and Knoll, 2002), thereby restricted the occurrence and evolution of eukaryotes via a bioinorganic bridge linking Mo to nitrogen availability.

Sulfur and nitrogen isotopic fractionation combined with the abundance of molybdenum (Mo) imply that nitrifying and denitrifying microbes were present before oxygen first began accumulating in the atmosphere (Garvin et al., 2009). Within a low oxygen atmosphere it would be difficult for non-nitrogen fixing organisms, such as eukaryotes, to obtain the fixed nitrogen required for synthesis of vital bio-molecules. Eukaryotes commonly assimilate fixed nitrogen from their surroundings (Anbar and Knoll, 2002; Porter, 2006; Garvin et al., 2009). Within nutrient limited conditions eukaryotes compete poorly with cyanobacteria and in modern oceans the growth of larger algae is facilitated by high nitrate levels (Malone, 1980, Lindell 1998). As a potentially multicellular prokaryote, rather than a eukaryotic alga, *Grypania* would likely be better equipped to deal with the likely nutrient stresses of Mesoproterozoic oceans.

Prior to ~1250 Ma eukaryotic algae preferred coastal and estuarine sites due to the proximity of these areas to nutrient and dissolved metal sources derived from rivers and upwelling on basin margins (Anbar and Knoll, 2002). If *Grypania* is indeed eukaryotic, its preservation in dominantly shallow water, lagoon to estuarine sediments (Walter et al., 1990; Kumar, 1995) is consistent with environments of lesser nutrient limitations. In sum, although environmental conditions may not have been inhibitory for evolution of multicellular macroscopic eukaryotes, neither would have necessarily been conductive to their widespread occurrence. The paucity of clearly eukaryotic features preserved for *Grypania* however suggests that a multicellular bacterial affinity best fits the present data.

6. Conclusions

Grypania is represented by a variety of morphologies from straight, to loosely coiled, to tightly coiled. The presence of possible holdfast structures and variety of coiling morphologies suggest that *Grypania* in life form was likely a benthic organisms shaped as an ovoid helix.

In fossil form, *Grypania* is preserved dominantly as faint discolorations on the shale surface or as shallow impressions into the shale matrix. Although organic content above background matrix is rarely preserved, *Grypania* occasionally contains early diagenetic pyrite, and likely some clay templating that indicates former presence of organic material.

This thesis suggests that *Grypania* features are best explained by the early diagenetic decomposition of a thin sheath of multicellular or coenocytic bacteria. Such an interpretation is also consistent with a growing understanding of Proterozoic oceanic and atmospheric evolution that, while not negating the possibility of a eukaryotic interpretation for *Grypania*, suggests protracted oxygenation of the oceans, nutrient limitation, and delayed onset of multicellular eukaryotic algae.

References

Anbar, A.D., Knoll, A.H., 2002. Proterozoic ocean chemistry and evolution: A bioinorganic bridge? Science 297, 1137-1142.

Anderson, H.E., Davis, D.W., 1995. U-Pb geochronology of the Moyie sills, Purcell Supergroup, Southeastern British Columbia: Implications for Mesoproterozoic geological history of the Purcell (Belt) basin. Canadian Journal of Earth Sciences 32, 1180-1193.

Arouri, K.R., Greenwood, P.F., and Walter, M.R., 1999. A possible chlorophycean affinity of some Neoproterozoic acritarchs. Organic Geochemistry 30, 1323-1337.

Bartley, J.K., 1996. Actualistic taphonomy of cyanobacteria: Implications for the Precambrian Fossil Record. Palaios 11, 571-586.

Bekker, A., Holland, H.D., Wang, P.L., Rumble, D., Stein, H.J., Hannah, J.L., Coetzee, L.L., Beukes, N.J., 2004. Dating the rise of atmospheric oxygen. Nature 427, 117-120.

Brenchly, P.J., Harper, D.A.T., 1998. Paleoecology: Ecosystems, Environments, and Evolution. Thompson Science London, UK. 432p.

Briggs, D.E.G., Moore, R.A., Shultz, J.W., Schweigert, G., 2005. Mineralization of soft-part anatomy and invading microbes in the horseshoe crab mesolimulus from the Upper Jurassic Lagerstatte of Nusplingen, Germany. Proceedings of the Royal Society of London Biological Sciences 272, 627-632.

Briggs, D.E.G., Bartels, C., 2010. Annelids from the Lower Devonian Hunsruumck Slate (Lower Emsian, Rhenish Massif, Germany). Palaeontology 53, 215-232.

Brocks, J.J., Logan, G.A., Buick, R., Summons, R.E., 1999. Archean molecular fossils and the rise of early eukaryotes. Science 285, 1033-1036.

Brocks, J.J., Buick, R., Logan, G.A., Summons, R.E., 2003. Composition and syngeneity of molecular fossils from the 2.78-2.45 billion year old Mount Bruce Supergroup, Pilbara Craton, Western Australia. Geochimica and Cosmochimica Acta 67, 4289-4319.

Butterfield, N.J., 1990. Organic preservation of non-mineralizing organisms and the taphonomy of the Burgess Shale. Paleobiology 16, 272-286.

Butterfield, N.J., 2000. Bangiomorpha pubescens n. gen., n. sp.: Implications for the evolution of sex, multicellularity, and the Mesoproterozoic/Neoproterozoic radiation of eukaryotes. Paleobiology 26, 386-404.

Butterfield, N. J., 2003. Exceptional fossil preservation and the Cambrian explosion. Integrative and Comparative Biology 43, 166-177.

Butterfield, N.J., 2009. Modes of pre-Edicaran multicellularity. Precambrian Research 173, 201-211.

Canfield, D.E., Thamdrup, B., Hansen, J.W., 1993. The anaerobic degradation of organic matter in Danish coastal sediments: Iron reduction, manganese reduction, and sulfate reduction. Geochimica et Cosmochimica Acta 57, 3867-3883.

Canfield, D.E., 1998. A new model for Proterozoic ocean chemistry. Nature 396, 450-453.

Chen, H., 1985. A typical model for the lead isotope evolution in the strata-bound deposits in China. Bulletin of the Yichang Institute of Geology and Mineral Resources 9, 105-116.

Crawford, A.R., Compston, W., 1970. The age of the Vindhyan System of Peninsular India. Quarterly Journal of the Geological Society 125, 251–371.

Crawley, J.C.W., 1964. Cytoplasmic fine structure in Acetabularia. Experiences in Cellular Research 35, 497-506.

Cuvellier, H., 1994. Pb-Pb and U-Pb geochronology of carbonate rocks: an assessment. Chemical Geology 115, 125-151.

Droser, M.L., Jensen, S., Gehling, J.G., 2002. Trace fossils and substrates of the terminal-Proterozoic-Cambrian transition: Implications for the record of early bilaterians and sediment mixing. Proceedings of the National Academy of Science, USA 99, 12572-12576.

Du R., Lifu, T., 1985. Algal macrofossils from the Quingbaikou System in the Yanshan Range of North China. Precambrian Research 29, 1906-1911.

Du, R., Lifu, T., et al., 1986. Discovery of Megafossils in the Gaoyuzhuang Formation of the Chancheng System, Jixian. Acta Geologica Sinica 60, 115-119.

Dutta, S., Steiner, S., Banerjee, S., Erdtmann, B.D., Jevankumar, and Mann, W., 2006. *Chuaria circularis from* the early Mesoproterozoic Suket Shale, Vindhyan Supergroup, India: Insights from light and electron microscopy and pyrolysis-gas chromatography. Journal of Earth Systems Science 115, 99-112.

Faegri, K. and Iverson, J., 1975. Textbook on Pollen Analysis. Third Edition. Munksgaard, Copenhagen; Blackwell Scienctific, Oxford Hafner Press. 296 p.

Falkowski, P. G. Raven J. A., 1996. Aquatic Photosynthesis. Blackwell Science, Malden, MA. 375 p.

Farquhar, J., Bao, H., Thiemens, M., 2000. Atmospheric influences of the Earth's earliest sulfur cycle. Science 289, 756-758.

Farquhar, J. Wing, B.A., 2003. Multiple sulfur isotopes and the evolution of the atmosphere. Earth and Planetary Science Letters 213, 1-13.

Gaines, R.R., Briggs, D.E.G, Yuanlong, Z., 2008. Cambrian Burgess Shale-type deposits share a common mode of fossilization. Geology 36, 755-758.

Garvin, J., Buick, R.R., Anbar, A.D., Arnold, G.L., Kaufman, A.J., 2009. Isotopic evidence for an aerobic Nitrogen cycle in the latest Archean. Science 323, 1045-1048.

Glaessner, M.F., 1987. Discussion about some worm like fossils. Precambrian Research 36, 353-356.

Gellatly, A.M., and Lyons, T.W., 2005. Trace sulfate in mid-Proterozoic carbonates and the sulfur isotope record of biospheric evolution. Geochimica et Cosmochimica Acta 69, 3813-3829.

Gerlach, D.C., Shirey, S.B., and Carlson, R.W., 1998. Neodymium isotopes in Proterozoic rocks. Eos 69, 1515.

Gregory, L.C., Meert, J.G., Pradhan, V., Pandit, M.K., Tamrat, E., Malone, S.J., 2006. A paleomagnetic and geochronologic study of the Majhgawan kimberlite, India: Implications for the age of the Upper Vindhyan Supergroup. Precambrian Research 149, 65-75.

Grey, K., Williams, I.R., 1990. Problematic bedding plane markings from the Middle Proterozoic Manganese Subgroup, Bangemall Basin, Western Australia. Precambrian Research 46, 307-328.

Han, T.M., Runnegar, B., 1992. Megascopic eukaryotic algae from the 2.1-billion-year-old Negaunee Iron-Formation, Michigan. Science 257, 232-235.

Harrison, J. E., 1972. Tectonic features of the Precambrian Belt basin and their influence on the post-Belt structures. U.S. Geological Survey Professional Paper 866. 15 p.

Hedges, J. I., Stern, J.H., 1984. Carbon and nitrogen determinations of carbonate-containing solids. Limnology and Oceanography 29, 657-663.

Hedges, S.B., Blair, J.E., Verturi, M.L., Shoe, J.L., 2004. A molecular timescale of eukaryotic evolution and the rise of complex multicellular life. BMC Evolutionary Biology 4, 1-9.

Hofmann H. J., Chen, J., 1981. Carbonaceous megafossils from the Precambrian (1800 Ma) near Jixian, northern China. Canadian Journal of Earth Science 18, 443-447.

Holland, H.D., 2006. The oxygenation of the atmosphere and oceans, Philosophical Transactions of the Royal Society 1470, 903-915.

Horodyski, R.J., 1993. Paleontology of Proterozoic shales and mudstones: examples from the Belt Supergroup, Chuar Group and Pahrump Group, western USA. Precambrian Research 61, 241-278.

Huffman, E.W.D. Jr., 1977. Performance of a New Automatic Carbon Dioxide Coulometer. Microchemical Journal 22, 567-573.

Hurtgen, M.T., Arthur, M.A., Suits, N., and Kaufman, A.J., 2002, The sulfur isotopic composition of Neoproterozoic seawater sulfate: Implications for a 'snowball earth': Earth and Planetary Science Letters, v. 203p. 413-430.Jahn, B.,

Javaux, E. J., Knoll A.H., Walter, M.R., 2003. Recognizing and interpreting the fossils of early eukaryotes. Origins of Life and Evolution of the Biosphere 33, 75-94.

Javaux, E. J., Knoll A.H., Walter, M.R., 2004. TEM evidence for eukaryotic diversity in mid-Proterozoic oceans. Geobiology 2, 121-132.

Kah, L.C., Lyons, T.W., Chesley, J.T., 2001. Geochemistry of a 1.2 Ga carbonate-evaporite succession, northern Baffin and Bylot islands: Implications for Mesoproterozoic marine evolution. Precambrian Research 111, 203-234.

Kah, L. C., Lyons, T.W., Frank, T.D., 2004. Low marine sulphate and protracted oxygenation of the Proterozoic biosphere. Nature 431, 834-838.

Karhu J.A., Holland, H.D., 1996. Carbon isotopes and the rise of atmospheric oxygen. Geology 24, 867-870.

Kasting, J.F., Toon, O.B., Pollack, J.B., 1988. How climate evolved on the terrestrial planets. Scientific American 258, 90-97.

Kasting, J.F. Seifert J.F., 2002. Life and the evolution of earth's atmosphere. Science 296, 1066–1067.

Kidder, D.L., Awramick, S.M., 1990. Acritarchs in lower greenshist facies argillite of the Middle Proterozoic Libby Formation, Upper Belt Supergroup, Montana. Palaios 5, 124-133.

Knoll, A.H., 1992. The early evolution of eukaryotes; a geological perspective. Science 256, 622-627.

Knoll, A.H., Carroll, S.B., 1999. Early animal evolution: Emerging views from comparative biology and geology. Science 284, 2130-2137.

Knoll, A.H., Javaux E.J., Hewitt, D., and Cohen, P., 2006. Eukaryotic organisms in Proterozoic oceans. Philosophical Transactions - Royal Society of London. Biological Sciences 361, 1023-1038.

Kumar, S., 1995. Megafossils from the Mesoproterozoic Rhotas Formation (the Vindhyan Supergroup), Katni area, central India. Precambrian Research 72, 171-184.

Kumar, S., 2001. Mesoproterozoic megafossil Chuaria-Tawuia association may represent parts of a multicellular plant, Vindhyan Supergroup, central India. Precambrian Research 106, 187-211.

Lamb, D. M., Awramik, S.M., Zhu, S., 2007. Paleoproterozoic compression-like structures from the Changzhougou Formation, China; eukaryotes or clasts? Precambrian Research 154, 236-247.

Lindell, D., Padan, E., Post, A.F., 1998. Regulation of ntcA expression and nitrate uptake in the marine synechococcus sp. Strain WH 7803. Journal of Bacterialogy 180, 1878-1886.

LoDuca, S.T., Behringer, E.R., 2009. Functional morphology and evolution of early Paleozoic dasycladacean algae (Chlorophyta). Paleobiology 35, 63-76.

Lu, S., Li, H., 1991. A precise U-Pb single zircon age determination for the volcanics of Dahongyu Formation, Chenchang System in Jixian. Bulletin of the Chinese Academy of Science 22, 137-146.

Lyons, T.W., Lupke, J.J., Schrieber, M.E., Zieg, G.A., 2000. Sulfur geochemical constraints on Mesoproterozoic restricted marine deposition: Lower Belt Supergroup, northwestern United States. Geochimica et Cosmochimica Acta 64, 427-437.

Lyons, T.W., Anbar, A.D., Severmann, S., Scott, C., Gill, B., 2009. Tracking euxinia in the ancient ocean: A multiproxy perspective and Proterozoic case study. Annual Review of Earth and Planetary Science 37, 507-534.

Mankiewitz, C., 1992. Obruchevella and other microfossils in the Burgess Shale: Preservation and affinity. Journal of Paleontology 66, 717-729.

Marshall, C.P., Javaux, E.J., Knoll, A.H., Walter, M.R., 2005. Combined micro-Fourier transform infrared (FTIR) spectroscopy and micro-Raman spectroscopy of Proterozoic acritarchs: A new approach to Paleobiology. Precambrian Research 138, 208-224.

Malone, T.C., 1980. Algal Size. In Morris. I. (ed) The physiological ecology of phytoplankton. Blackwell Scientific Publishers, London. 433-464.

Moczydlowska, M., Willman, S., 2009. Ultrastructure of cell walls in ancient microfossils as a proxy to their biological affinities. Precambrian Research 173, 27-38.

Mueller, P.A., Heatherington, A.L, Kelly, D.M., Wooden, J.L., Mogk, D.W., 2002. Paleoproterozoic crust within the Great Falls tectonic zone: Implications for assembly of southern Laurentia. Geology 30, 127-130.

Neilson, P.L., 2006. Size-dependent growth rates in eukaryotic and prokaryotic algae exemplified by green algae and cyanobacteria: comparisons between unicells and colonial growth forms. Journal of Plankton Research 28, 489-498.

Oehler, D.Z., 1977. Pyrenoid-like structures in late Precambrian algae from the Bitter Springs Formation of Australia. Journal of Paleontology 51, 885-901.

Orr, P.J., Briggs, D.E.G., Kearns, S.L., 1998. Cambrian Burgess Shale animals replicated in clay minerals. Science 281, 1173-1175.

Orr, P.J., Kearns, S.L., Briggs, D.E.G., 2002. Backscattered Electron Imaging of Fossils Exceptionally Preserved as Organic Compressions. Palaios 17, 110-117.

Orr, P.J., Kearns, S.L., Briggs, D.E.G., 2009. Elemental mapping of exceptionally preserved 'carbonaceous compression' fossils. Paleogeography, Paleoclimatology, Paleoecology 277, 1-8.

Payne, J.L., Boyer, A.G., Brown, J.H., Finnegan, S., Kowalewski, M., Krause, R.A., Lyons, S.K., McClain, C.R., McShea, D.W., Novack-Gottshall, P.M., et al., 2009. Two-phase increase in the maximum size of life over 3.5 billion years reflects biological innovation and environmental opportunity. Proceedings of the National Academy of Sciences USA 106, 24-27.

Peng, Y., H. Bao, and Yuan, X., 2009. New morphological observations for Paleoproterozoic acritarchs from the Chuanlinggou Formation, North China. Precambrian Research 168, 223-232.

Porter, S. M., 2006. The Proterozoic Fossil Record of Heterotrophic Eukaryotes, in Xiao, S., Kaufman, A.J. (Eds.), Neoproterozoic Geobiology and Paleobiology. Springer, Dordrecht 1-21.

Poulton, S.W., Canfield, D.E., Fralick, P., 2004. The transition to a sulfidic ocean ~1.84 billion years ago. Nature 431, 173-177.

Ray, J.S., Veizer, J., Davis, W.J., 2003. C, O, Sr, and Pb isotope systematics of carbonate sequences of the Vindhyan Supergroup, India: age, diagenesis, correlations and implications for global events. Precambrian Research 121, 103-140.

Raiswell, R., Canfield, D.E., 1998. Sources of iron for pyrite formation in marine sediments. American Journal of Science 298, 219-245.

Raymond, P.E., 1935. Pre-Cambrian life. Geological Society of America Bulletin 46, 375-392.

Reed, S.J.B., 2005. Electron microprobe analysis and scanning electron microscopy in geology. University Press Cambridge. Cambridge, UK. 189 p.

Runnegar, B., 1991. Precambrian oxygen levels estimated from the biochemistry and physiology of early eukaryotes. Global and Planetary Change 5, 97-111.

Samuelsson, J., Butterfield, N.J., 2001. Neoproterozoic fossils from the Franklin Mountains, northwestern Canada: stratigraphic and palaeobiological implications. Precambrian Research 107, 235-251.

Sarangi, S., Gopalan, K., Kumar, S. 2004. Pb-Pb age of earliest megascopic, eukaryotic alga bearing Rohtas Formation, Vindhyan Supergroup, India: implications for Precambrian atmospheric oxygen evolution. Precambrian Research 132, 107-121.

Schiffbauer, J., Yin, L., Bodnar, R.J, Kaufman, A.J., Meng, F., Hu, J., Shen, B., Yuan, X., Bao, H., Xiao, S., 2007. Ultrastructural and geochemical characterization of Archean-Paleoproterozoic graphite particles: Implications for recognizing traces of life in highly metamorphosed rocks. Astrobiology 7, 684-704.

Schiffbauer, J., Xiao, S., 2009. Novel application of focused ion beam electron microscopy (FIB-EM) in preparation and analysis of microfossil ultrastructure: A new view of the complexity of early eukaryotic organisms. Palaios 24, 616-626.

Schneider, D.A., Brickford, M.E., Cannon, W.F., Schulz, K.J., Hamilton, M.A., 2002. Age of volcanic and syndepositional iron formations, Marquette Range Supergroup: implications for the tectonic setting of the Paleoproterozoic iron formations of the Lake Superior region. Canadian Journal of Earth Science 39, 999-1012.

Schopf, J.W., 1994. Disparate rates, differing fates: Tempo and mode of evolution changed from the Precambrian to the Phanerozoic. Proceedings of the National Academy of Science, USA 91, 6735-6742.

Schopf, J.W., Kudryavtsev, A.B., Tripathi, A. 2002. Laser-Raman imagery of Earth's earliest fossils. Nature 416, 73-76.

Schopf, J.W., Kudryavtsev, A.B., Agresti, D.G., Wdowiak, T.J., Czaja, A.D. 2005. Raman imagery: a new approach to assess the geochemical maturity and biogenicity of permineralized Precambrian Fossils. Astrobiology 5, 333-371.

Schouten, S., W., Klein Breteler, C.M., Blokker, P., Nelleke, S., Rijpstra, I.C., Grice, K., Baas, M., and Sinninghe Damste, J.S., 1998. Biosynthetic effects on the stable carbon isotopic compositions of algal lipids: implications for deciphering the carbon isotopic biomarker record. Geochimica et Cosmochimica Acta 62, 1397-1406.

Sears, J.W., Chamberlain, K.R., Buckley, S.N., 1998. Structural and U-Pb geochronological evidence for 1.47 Ga rifting in the Belt Basin, western Montana. Canadian Journal of Earth Sciences 35, 467-475.

Sharma, M., Mishra, S., Dutta, S., Banjeree, S., Shukla, Y., 2009. On the affinity of *Chuaria-Tawuia* complex: A multidisciplinary study. Precambrian Research 173, 123-136.

Sharma, M., Shukla, Y. 2009. Taxonomy and affinity of early Mesoproterozoic megascopic helically coiled and related fossils from the Rohtas Formation, the Vindhyan Supergroup, India. Precambrian Research 173, 105-122.

Sherman, L. S., Waldbauer, J.R., and Summons, R.E., 2007. Improved methods for isolating and validating indigenous biomarkers in Precambrian rocks. Organic Geochemistry 38, 1987-2000.

Soni, M.K., Chakraborty, S., Jain, V.K., 1987. Vindhyan Supergroup, a review. Geological Society of India Memoir, 87-118.

Srivastava, P., Bali, R., 2006. Proterozoic carbonaceous remains from the Chorhat Sandstone: oldest fossils of the Vindhyan Supergroup, Central India. Geobios 39, 873-878.

Summons, R. E., Powell, T.G., Boreham, C.J., 1988. Petroleum geology and geochemistry of the middle Proterozoic McArthur Basin, northern Australia; III, Composition of extractable hydrocarbons. Geochimica et Cosmochimica Acta 52, 1747-1763.

Summons, R.E., Albrecht, P., McDonald, G., Molodowan, J.M., 2008. Molecular Biosignatures. Space Science Reviews 135, 133-159.

Sun, W., 1987. Paleontology and biostratigraphy of late Precambrian macroscopic colonial algae: *Chuaria* Walcott and *Tawuia* Hoffmann. Palontographica , 109-139.

Talyzina, N.M., 2000. Ultrastructure and morphology of *Chuaria circularis* (Walcott, 1899) Vidal and Ford (1985) from the Neoproterozoic Visingso Group, Sweden. Precambrian Research 102, 123-134.

Taylor, K.G., Curtis, C.D., 1995. Stability and facies association of early diagenetic mineral assemblages: An example from a jurasic ironstone-mudstone succession, U.K. Journal of Sedimentary Research A65, 358-368.

Traverse, A., 2008. Paleopalynology. Second edition. Springer, Dordrect, Netherlands 813p.

Tribovillard, N., Lyons, T.W. Riboulleau, A., and Bout-Roumazeilles V., 2008. A possible capture of molybdenum during early diagenesis of dysoxic sediments. Bulletin de la Societe Geologique de France 179, 3-12.

Vidal, G., 1989. Are late Proterozoic carbonaceous megafossils: metaphytic algae or bacteria? Lethaia 22, 375-379.

Vidal, G., Moczydlowska, M., Rudavskaya, V., 1993. Biostratigraphical implications of a *Chuaria-Tawuia* assemblage and associated acritarchs from the Neoproterozoic of Yakutia. Paleontology 36, 387-402.

Vorhies, J.S., and Gaines, R.R., 2005. Carbonate concretions from the Wheeler Formation preserve evidence suggesting microbial reduction of structural (FeIII) from clay minerals in Cambrian sediments. Geological Society of America Abstracts and programs 37, 258.

Walcott, C.D., 1899. Precambrian fossiliferous formations. Geological Society of America Bulletin 10, 199-244.

Walter, M.R., Oehler J.H., Oehler, D.Z., 1976. Megascopic algae 1300 million years old from the Belt Supergroup, Montana; a reinterpretation of Walcott's *Helminthoidichnites*. Journal of Paleontology 50, 872-881.

Walter, M.R., Du, R., Horodyski, R.J., 1990. Coiled carbonaceous megafossils from the middle Proterozoic of Jixian (Tianjin) and Montana. American Journal of Science 290-A, 133-148.

Wand, M.P., 1997. Data based choice of histogram bin width. American Statistician 51, 59-64.

Woese, C.R., Kandler, O. Wheelis, M.L., 1990. Towards a natural system of organisms: proposal for the domains Archaea, Bacteria, and Eucarya. Proceedings of the National Academy of Sciences 87, 4576-4579.

Xiao, S., Knoll, A.H., 2000. Phosphatized animal embryos in the Neoproterozoic Doushantuo Formation at Weng'An, Guizhou, south China. Journal of Paleontology 74, 767-788.

Xiao, S., Dong, L., 2006. Morphological and Ecological History of Proterozoic Macroalgae, in Xiao, S., Kaufman, A.J., (Eds.), Neoproterozoic Geobiology and Paleobiology, pp. 59-70.

Zhang, W., Walter, M.R., 1992. Late Proterozoic and early Cambrian microfossils and biostratigraphy, northern Anhui and Jiangsu, central-eastern China. Precambrian Research 57, 243-323.

Zhang, X. L., Hua, H., Reitner, J., 2006. A new type of Precambrian megascopic fossils: the Jixian biota from northeastern China. Facies 52, 169-181.

Appendix 1: Field Images

Items in Appendix 1 zip file

*Contact Linda Kah at lckah@utk.edu or the EPS department for full appended data with bound copy of thesis

Folder 1: Field Pictures

104 images from Greyson Shale locality

Appendix 2: Low Power Microscopy

Items in Appendix 2 zip file

*Contact Linda Kah at lckah@utk.edu or the EPS department for full appended data with bound copy of thesis

Folder 1: Gaoyuzhuang Formation
- 11 items
  - GAO-1 to GAO-11

Folder 2: Greyson Shale
- 230 items
  - BS-A to BS-H
  - GS-C1
  - GS-D1
  - GS-F1 to GS-F30
  - GS-M1 to GS-M13
  - GS-P1 to GS-P26
  - GS-PCA to GS-PCZ
  - GS-U1 to GS-U5
  - HH-1 to HH-7
  - WG-1 to WG-6

Folder 3: Microscope Images
- 28 items
  - BS-B to IND-C

Folder 4: Negaunee Iron Formation
- 6 items
  - NG-1 to NG-4

Folder 5: Rohtas Limestone
- 16 items
  - IND-A to IND-L

Appendix 3: Morphology Measurements

Items in Appendix 3 zip file

*Contact Linda Kah at lckah@utk.edu or the EPS department for full appended data with bound copy of thesis

Frequency distributions plotted from data

- Number of coils at 11 and 15 bins
- Coil diameter at 6 and 15 bins
- Ribbon length at 18 and 25 bins
- Ribbon width at 11 and 15 bins

Size frequency measurements in Excel

Appendix 4: Scanning Electron Microscopy

Items in Appendix 4 zip file
*Contact Linda Kah at lckah@utk.edu or the EPS department for full appended data with bound copy of thesis

Picture of sample in ESEM chamber

Notes from ESEM word document

Folder 1: Composite Images -18 items

HH-1 BSD and SED
IND-B BSD and SED
IND-L BSD and SED
IND-C BSD and SED
GAO-7 BSD and SED
GAO-8 BSD and SED
GS-F30 BSD and SED
GS-F23 BSD

Folder 2: Elemental Maps - 57 maps at various magnifications

BS-C
GAO-3
GAO-4
GAO-6
GAO-8
GS-D1
GS-F12
GS-F30
GS-M5
GS-P27
GS-PCL
GS-PCZ
GS-S23
GS-U2
HH-1
HH-2
HH-3
HH-4
HH-5
IND-B
IND-C
IND-BC
IND-L

Folder 3: ORNL Data

Chinese Matrix Folder (CM)

Montana Folder

Thin Section 1 Folder

Elemental mapping of ribbon impressions in thin section

Thin Section 2 Folder

BSD images of *Grypania* ribbons

10 images labeled J09988 to J09996

Folder 4: Raw Data

Data from observed samples

BS-C
GAO-2
GSO-3
GAO-4
GAO-6
GAO-7
GAO-8
GAO-9
GS-D1
GS-F23
GS-F30
GS-M5
GS-P27
GS-PCL
GS-PCL'
GS-PCY
GS-PCZ
GS-S7
GS-S23
GS-U2
HH-1
HH-2
HH-3
HH-4
HH-5
HH-7
IND-A1
IND-B
IND-C'
IND-L
NG-2

Appendix 5: Geochemistry

Items in Appendix 5 zip file

*Contact Linda Kah at lckah@utk.edu or the EPS department for full appended data with bound copy of thesis

Folder 1: Coloumetric data
- Organic carbon measurements
- Inorganic carbon measurements

Folder 2: XRD data
- Act Labs Report and raw data

Folder 3: K-AR data
- Act Labs Report

Folder 4: Thin sections
- Pictures of TS-1 and TS-2 before thin sections were made

Folder 5: Grain Sizes
- Images grain sizes were measured from
- Data sheet

Vita

Miles is a born and raised Georgia boy. Growing up he was involved in the Boy Scouts of America and proudly earned the highest rank of Eagle Scout in 2006. Miles started his geological education at Georgia Perimeter College where he earned his Associate's degree in 2005. Miles then graduated with his Bachelor's degree in Geology from the University of Georgia in 2008. This thesis fulfills the last of the requirements for the Master of Science degree from the University of Tennessee. Miles plans on obtaining employment within the geological industry and one day hopes to return to higher education and pursue a PhD.